C6-144/32 Copy._____

PHOTODETECTOR EVALUATION FOR CELESTIAL SENSING

JPL Contract 951191

January 20, 1966

AUTONETICS
A DIVISION OF NORTH AMERICAN AVIATION, INC.

This work was performed for the Jet Propulsion Laboratory, California Institute of Technology, pursuant to a subcontract issued under Prime Contract NAS 7-100 between the California Institute of Technology and the United States of America represented by the National Aeronautics and Space Administration.

CONTENTS

LIST OF FIGURES

1. INTRODUCTION

As a part of the continuing effort to reduce the size, weight, and power requirements of components utilized in space navigation systems, it is desirable to replace vacuum type photodetection devices with small and highly reliable solid state photodetectors. To accomplish this purpose, Autonetics has developed a vacuum deposited thin film form of photoconducting cadmium sulfide. In the past, the sintered form of cadmium sulfide has been used for photodetectors in space navigation. However, sintered cadmium sulfide photodetectors have several disadvantages. One of the major disadvantages for application in space vehicles is that the detectors will not survive the thermal sterilization requirements for a package which may contact other planets. Other disadvantages of this form of cadmium sulfide includes a high degree of instability with temperature variances and the fact that any degree of water vapor will degrade the performance of these detectors. The latter effect requires that the detector be hermetically sealed immediately following fabrication.

The object of the evaluation conducted under this contract was to determine the characteristics of vacuum deposited cadmium sulfide under environmental conditions required for thermal sterilization and, ultimately, prolonged operation in outer space.

Since many applications of photodetectors require the use of two detectors operated in a bridge configuration such that the output of one detector is balanced against a second detector, the long term null stability of two detectors operated in this manner was of major concern. This has been evaluated under wide ranges of illumination and temperatures.

In addition to the investigation of the long term null stability and thermal sterilization cycle survival, several other significant characteristics of these detectors have been investigated. Maximum operating limits have been determined for bias voltage while in the dark and power dissipation under typical light level conditions. Since it is possible that in some applications, such as a sun sensor, the detectors will be exposed to extremely high light levels, a test was conducted to determine if the detector can survive for short periods of time at illumination levels as high as 10^{+6} foot-candles. Data are also reported on rise and fall time measurements in this material as a function of illumination levels and temperature. The study was completed with tests to determine the effects of a high vacuum environment and the measurement of light memory or hysteresis effects of prolonged storage in either the light or dark.

The results of this evaluation are described and illustrated in the following sections. In summary, some of the conclusions drawn from this evaluation are that detectors fabricated from this material will survive the thermal sterilization cycle. The measured null stability is adequate for most immediate application of nulling type detectors. All other tests performed indicate that this material could successfully be used for space guidance applications.

2. PHOTODETECTOR DESCRIPTION

The detectors used throughout this evaluation consist of a mixture of cadmium sulfide (CdS) and cadmium selenide (CdSe) vacuum deposited on glass substrates 0.25 inch square.

The electrodes for these detectors were initially nickel vacuum deposited over an extremely thin film of indium for ohmic contact. It was later found that the nickel would crack and peel at temperatures required for thermal sterilization so later detectors had electrodes of gold replacing the nickel.

The detector configuration was a serpentine design with the width of the active areas 0.005 inch and the length of each leg of the sepentine approximately 0.150 inch. The separation between each of twenty elements of the serpentine is 0.005 inch.

3. THERMAL STERILIZATION CYCLE SURVIVAL

One of the key advantages that a vacuum deposited thin film CdS photoconductor should have over a photoconductor fabricated with the sintered form of CdS is that it should be able to survive the thermal sterilization requirements of certain space vehicle applications. Thermal sterilization requires that all components of the vehicle must remain operational after being heated to a temperature of 145° C and held at that temperature for a period of 36 hours then cooled to room temperature. This cycle to be repeated three times.

The purpose of this portion of the program was to evaluate Autonetics vacuum deposited CdS photodetectors to verify their ability to survive a sterilization cycle of this nature.

All of the sterilization cycle evaluations discussed below were conducted in the following manner. An oven was preheated to 145° C measured by a mercury thermometer inserted in the oven adjacent to the position of the detector. The oven was constantly maintained at this temperature to within $\pm 2^{\circ}$ C. The detectors to be tested were placed on a glass tray and inserted directly into the preheated oven. After the 36 hour heating period the detectors were taken directly from the hot oven to room temperature without a slow cooling. In both the case of insertion and removal of the detectors from the oven the thermal shock was considerable.

The initial detectors fabricated for this program used nickel electrodes vacuum deposited over an extremely thin coating of indium to achieve an ohmic contact to the CdS. In the first sterilization tests two of these detectors were placed in the heated oven and left for 36 hours. Upon removal visual inspection showed that the nickel electrodes had cracked and peeled away from the CdS film in large areas on both detectors. This was apparently due to the fact that the coefficient of thermal expansion of nickel is about three times larger than that of CdS and that nickel is a relatively hard and brittle material as compared to other electrode materials. The combination of these two factors leads to the cracking and peeling of the electrode upon heating. Later in the program another detector with nickel was tested, however, the detector was placed in the oven when it was at room temperature. The temperature was raised very slowly and after the 36 hours cooled very slowly to determine if the cracking was due to the thermal shock rather than the prolonged high temperature. Inspection of this device showed the same cracking and peeling as the previous nickel units.

To eliminate this problem new detectors were fabricated with electrodes of gold deposited over the thin indium film. Gold was used in this case since it is much more malable than nickel and would not have the tendancy to crack.

A plot of photocurrent versus illumination was made on two gold electrode detectors prior to placing them in the preheated oven. After heating 36 hours the detectors were removed and the photocurrent-illumination characteristic was remeasured. Curves A in Figures 1 and 2 illustrate the characteristics prior to heating and Curves B in the two Figures represent the characteristics after heating. Comparison of Curves A and B shows an increase in resistance of the detectors during heating which is small at high illuminations and gets increasingly larger as the illumination decreases. After taking these data, the detectors were cycled through the same heating procedure and remeasured. This is illustrated by Curves C in Figures 1 and 2. It should be noted that Curves C and B are the same to within the error of the test. The heat cycle was repeated two more times on both detectors and the characteristics measured after each cycle. Curves D and E represent these data. The variations seen in Curves B, C, D and E are within the experimental error of the test. It should be pointed out that the spread in the curves increases as the light level decreases or as the detectors become large value resistances. At approximately 10^{-3} foot-candles the detector impedance is the same order as its surroundings and data taken at this point and below are not felt to be significant or accurate.

The above data indicate that there is some type of ageing process which takes place during the first heating cycle. This, however, seems to go to completion within the first 36 hours and further heating cycles have no effect on the detector characteristics.

The conclusions drawn from this test are that if the initial heating is incorporated into the fabrication process, these detectors will survive the thermal sterilization cycle.

4. LONG TERM NULL STABILITY

One of the basic requirements for the use of photodetectors in an application where one detector is balanced against another, is that the ultimate stability of the null of the pair remains well within the accuracy requirements of the system. As a part of this program, Autonetics thin film photodetectors were evaluated to determine the long term null stability of this type of detector. This evaluation was conducted over an illumination range from 0.01 foot-candles to 100 foot-candles and over a temperature range from -14°F to 120°F. In the following, the technique used for determining null stability is described and a detailed analysis of the errors in this technique is included.

The evaluation of the null stability was accomplished by arranging detectors in a bridge circuit as shown in Figure 3. The voltage applied to the bridge was 3.000 volts. Z_2 was varied until 1.500 volts were applied across each leg. Z_4 was then adjusted to give a zero reading on Recorder A (system drift). Z_5 was then adjusted to give a zero reading on Recorder B (absolute cell drift). Z_8 was then adjusted to give a zero reading on Recorder C (relative cell drift). A time recording of these three outputs was taken simultaneously with the recording of the output of an iron-constantan thermocouple to monitor the cell temperature. All resistors in the bridge were wire-wound. The recorder used was a four-channel Sanborn 150 with 5 megohm input impedance. Cell bias was obtained from a Kepco regulated dc supply (Model CK18-3M). Controlled temperature enclosure was a Delta type Non-Linear Systems Oven.

In all cases the system drift was negligible and is not included in the following data. All drift data are plotted in terms of percent. The percentages as quoted are obtained from the equation

$$\left(\frac{\Delta R}{R}\right) = -4\left(\frac{\Delta V}{E}\right) \tag{1}$$

which is derived below. Consider the circuit shown in Figure 3. Z_2, Z_4, Z_5 and Z_8 are adjusted at the beginning of the test such that the voltage drops across Z_1, Z_2, Z_3, Z_4, Z_5 Cell I, Z_6, Z_7 Cell II and Z_8 are all equal to $\frac{1}{2}E$. This makes $V_1 = V_2 = 0$ at the beginning of the test. The resistances of Recorders A, B and C are assumed to be much greater than the resistance of the circuit elements. The equation for Loop 1 is

$$V_1 = \frac{E}{2} - \frac{EZ_6}{Z_6 + Z_8} \tag{2}$$

Taking the derivative

$$\frac{dV_1}{dZ_6} = 0 - \left[\frac{(Z_6 + Z_8)\,E - EZ_6}{(Z_6 + Z_8)^2} \right] \tag{3}$$

$$\frac{dV_1}{dZ_6} = - \frac{EZ_8}{(Z_6 + Z_8)^2} \tag{4}$$

If we assume that $dZ_6 \ll Z_6$, we may make the following substitutions:

$$Z_6(t) + Z_8 \approx 2Z_6 \tag{5}$$

thus,

$$\frac{dV_1}{dZ_6} = - \frac{EZ_6}{(2Z_6)^2} \tag{6}$$

$$= \frac{-E}{4Z_6} \tag{7}$$

or

$$\frac{dZ_6}{Z_6} = - \frac{4dV_1}{E} \quad [\text{absolute drift}] \tag{8}$$

Since we started with the initial condition that $V_1 = 0$, then $V_1 = dV_1$ where V_1 is that shown by Recorder B. Thus,

$$\text{Percent Absolute Drift} = \frac{-4\,(\text{Reading on Recorder B})}{(\text{Bridge Bias})}\,(100) \tag{9}$$

The equation for Loop 2 is

$$V_2 = \frac{EZ_6}{Z_6 + Z_8} - \frac{EZ_7}{Z_7 + Z_8} \tag{10}$$

$$dV_2 = \frac{\partial V_2}{\partial Z_6}\,dZ_6 + \frac{\partial V_2}{\partial Z_7}\,dZ_7 \tag{11}$$

$$= \frac{EZ_8}{(Z_6 + Z_8)^2}\,dZ_8 - \frac{EZ_8}{(Z_7 + Z_8)^2} \tag{12}$$

Making similar approximations to those above, this equation reduces to

$$dV_2 = \frac{E}{4Z_6}\, dZ_6 - \frac{E}{4Z_7}\, dZ_7 \qquad (13)$$

$$\frac{4dV_2}{E} = \frac{dZ_6}{Z_6} - \frac{dZ_7}{Z_7}\ [\text{relative drift}] \qquad (14)$$

Again, since $V_2 = 0$ at $t = 0$, we have $dV_2 = V_2$. Thus,

$$\text{Percent Relative Drift} = \frac{4\ (\text{Reading on Recorder C})}{(\text{Bridge Bias})}\ (100)$$

The null stability evaluation was initiated by selecting two detectors, JPL-6 and JPL-24 which had closely matched photocurrent versus illumination characteristics. Detector JPL-6 was fabricated with nickel electrodes and JPL-24 had gold electrodes. Tests were begun at 1 foot-candle and 120°F. Results of this test are shown in Figure 4. As is illustrated in this figure the relative drift of the two detectors reached a peak of approximately 12 percent at the end of 48 hours. It did appear that this drift did tend to level out substantially during the last 24 hours. For the second test the illumination was held at the same level and the temperature reduced to 100°F. These data are given in Figure 5. It is significant that in this case the relative drift remained under 2 percent for the entire 48 hours.

Chronologically it was at this point in time that the effect of the first thermal sterilization cycle (Section 3) was discovered. This leads to the hypothesis that the large drift shown on the first test was the same type of effect seen in the first sterilization cycle.

Figure 5 is also significant since it illustrates a period of time where due to a malfunction the temperature decreased substantially from the operating temperature and was only slightly reflected in the relative drift recording.

Figures 6, 7 and 8 represent data taken at the same illumination and temperatures of 80°F, 55°F and 32°F respectively. These data show typical relative drifts of 2 to 4 percent.

Thermal sterilization tests which had been going on simultaneously with the drift tests had shown a definite stabilization of characteristics after the first heating cycle. Based on this it was decided to cycle detectors JPL-6 and 24 through the first heating to determine if they would stabilize even further than they had during the first drift run at 120°F.

This was done and the next data were taken at the 1 foot-candle illumination level and at 0°F. Figure 9 illustrates the results of this test. It appears from these data that no further "ageing" of the detectors was accomplished. However, JPL-6 which had nickel electrodes was damaged in the heating cycle and the electrode peeled off the CdS at the end of 32 hours of this test.

In the next series of tests the illumination level was reduced to 0.01 foot-candle and data were taken at each of the temperatures used on the 1 foot-candle tests. Detector JPL-6 was replaced with a new unit, JPL-28, which had gold electrodes and was cycled through the first sterilization heating prior to drift tests.

Several problems arose in this series. First the detector impedance was sufficiently high that wirewound resistors could not be used conveniently. These were replaced with carbon units which were placed outside the temperature chamber. The 0.01 foot-candle illumination was achieved by reducing the voltage on the lamp.

Figure 10 shows data taken at this illumination at 120°F. Immediately noticable is the large variations in the absolute drift of JPL-28, (+20 percent to -20 percent) while at the same time the relative drift of two detectors remained in the 4 to 6 percent region.

It was felt that this may be due to the low voltage used on the bias lamp and consequentially small fluctuations in supply voltage would result in large fractional light level variations. To verify this an experiment was conducted where the lamp bias was purposely varied and the absolute and relative drifts were monitored as a function of this variation. These results are given in Figure 11 and indicate this is probably the reason for the large variations in absolute drift in the previous test.

To eliminate this effect in future tests, the lamp bias voltage was increased and a neutral density filter was placed between the lamp and the detectors. To accommodate this modification the lamp was moved outside the temperature chamber and the detectors were illuminated through the window in the chamber.

Low light level tests at 100°F, 80°F and 55°F are shown in Figures 12, 13, and 14 respectively. These tests show essentially the same low value of relative drift as earlier tests. Figure 15 shows data taken at 30°F. This test resulted in a large variation for the first 12 to 14 hours then settled out to small fluctuations for the remainder of the test. It was found that this was the result of water vapor condensing on the window and was eliminated in future low temperature tests by coating the window with a thin film of silicone grease.

The lowest temperature test at 0.01 foot-candle was conducted at -14°F rather than 0°F, see Figure 16. At one point in this test, the CO_2 tanks ran dry and the temperature inside the controlled enclosure reached room temperature. When the temperature was again reduced to -14°F, the amount of drift returned approximately to the same value of drift recorded just before the large temperature change. For the last recording, the amplifier used in conjunction with the thermocouple failed to function properly. As a result, a concurrent temperature recording was not taken.

The last data taken is shown in Figure 17 where the illumination was 100 foot-candles and the temperature was 100°F. This is typical of other data. The maximum relative drift was 2.3 percent.

5. MAXIMUM OPERATING LIMITS

Tests were conducted to determine the maximum operating limits of detectors of this configuration. Of interest was the maximum bias voltage which could be applied in the dark and the maximum power dissipation. For the later test the illumination level was held constant at 150 foot-candles.

A circuit diagram illustrating the laboratory setup for determining maximum power dissipation and maximum bias voltage in the dark is given in Figure 18. For the bias voltage test, switch S2 was left open as shown in Figure 18. The DPDT switch, S1, was initially placed in position 1. This biased the photocell at 1.50 volts dc and applied a voltage across Lamp #1 which gave it a filament temperature of 2900° K. A neutral density filter was placed between Lamp #1 and the photocell, subjecting the photocell to some known illumination. The current through the photocell, I, was then measured. This process was repeated for two other illuminations. The illuminations used for these tests were 10, 1.0, and 0.1 foot-candles. After the 0.1 foot-candle current measurement, S1 was opened and the photocell placed in the dark for five minutes. This five minute "decaying" period was more or less a standard so that approximately the same current was flowing through the photocell when the different values of V were applied across the photocell. At the end of the decaying period, S1 was switched to position 2. Prior to this, V had been varied so that the photocell would be subjected to some predetermined applied voltage, V, when S1 was placed in position 2. After the photocell had been biased at V for five additional minutes, S1 was returned to position 1. Three more current measurements made under the illuminations mentioned above were compared with the initial current values to detect any possible change in cell characteristics. This entire procedure was repeated several times with larger values of V until the cell exhibited a complete failure. The failure mode for the detector was an arc across the detector at two points simultaneously when the applied voltage reached 300 volts.

Some interesting phenomena were observed during the above test. First, the photocell current, I, became "noisy" when V reached approximately fifty volts. This was probably due to the initiation of a space-charge-limited current through the photocell. Second, with V approximately equal to eighty volts, the milliammeter revealed occasional "pulse-like" increases in current with an immediate return to the steady-state current level. The pulses became more frequent as V became larger. The increase in the magnitude of the current during these pulses was on the order of thirty to fifty percent. These pulses

might be due to electrical discharges across the surface of the photocell. However, no visible damage could be detected when the photocell was observed under a microscope after it had been subjected to a treatment of V = 140 volts.

For the power dissipation limit test, S2 (in Figure 18) was closed. The only difference between this test and that above is that here, the photocell was subjected to the excess voltages while under a 150 foot-candle illumination, and there was no five minute waiting period for the dark current to decay. One phenomena noted from this test was that as V became larger, the current decayed more slowly to the steady state 1.5 volt level when S1 was placed in position 1. The results of these tests are recorded in Table 1. The largest voltage which the photocell survived along with the current measured for that voltage and the failure voltage are given.

Table 1. Results of Bias Voltage and Power Dissipation Tests

Limit Test	Photocell	Largest Survival Characteristics		Failure Voltage (volts)
		Voltage (volts)	Current (amps)	
Maximum bias voltage	JPL-36	275	1.8×10^{-9}	300
Maximum power dissipation	JPL-24	80	1.5×10^{-8}	100
		1.2 watts		

Since one application of detectors of this type would be for sun sensors a test was performed to determine of the detector would function at extremely high illumination levels. The maximum illumination used in this test was 10^5 foot-candles.

The results of the high illumination test are given in Figure 19. The cell was biased with 1.50 volts dc. The lamp employed was a fused Sylvania quartz-iodine lamp, DWY, and was operated at 115 volts ac. The lamp had a vilament temperature of 3400°K. The 10^5 foot-candles illumination required placing the photocell approximately 1.6 inches from the lamp. This short distance subjected the cell to intense heat which was hot enough that the cement on the back of the substrate

began to decompose during the five seconds required to take an accurate reading. Two other readings were taken with this same lamp to compare with earlier conductivity vs illumination values taken for the same cell. The slight differences observed for the two sets of readings at 10^3 and 10^4 foot-candles is due to the fact that the Sylvania lamp had a coil type filament at 3400°K while the earlier data were taken with a ribbon type filament at 2900°K. From all indications, no damage could be detected as a result of the high illumination.

6. RISE AND FALL TIMES

The rise and fall times of this material have been measured as a function of bias illumination, chopped signal illumination and temperature. It should be noted here that the rise and fall times of the thin film material can be adjusted within limits by variation of vacuum deposition parameters. The values measured here are typical of those previously measured for material similar to the type of material used to fabricate the test cells.

Figures 20, 21 and 22 represent the data taken at three temperatures (-8°F, 72°F, 138°F) and eight combinations of bias and signal illumination. The conditions of bias and signal illuminations are determined by referencing the letter of each curve to the matrix shown in each figure. For instance curve H represents a 0.01 foot-candle bias illumination and a 0.01 foot-candle chopped signal illumination.

The conditions for this experiment consisted of a detector biased at 1.5 volts being exposed to two 2900°K tungsten light sources one of which was shuttered. The illumination levels of each were adjusted by the distance of the light source and with neutral density filters. The rise and fall times were measured on an oscilloscope by recording the times required for the signal to rise to 63 percent of the final level and fall to 37 percent its initial level.

In analyzing these data an interesting fact is seen. Particularly for combinations of low light levels the rise time increases as the temperature is raised from 70°F to 138°F. The magnitude of this effect seems to be more a function of the bias illumination than the signal illumination. This is shown quite clearly by comparison of Curves A, B, C, D, E and F. Curve G seems to be an anomoly to this and no explanation for this is available. The effect is shown to a much smaller extent in the fall time data, however, Curves A, D, E and F do show the same effect.

7. VACUUM ENVIRONMENT SURVIVAL

For the vacuum environment test, a detector was mounted on insulating standoffs inside an unpainted aluminum container, Figure 23. A GE-605 lamp was also installed inside the container. A hole was drilled through the glass envelope of the lamp to prevent it from bursting when subjected to the low pressures involved with this test. The container was wrapped with aluminum foil to minimize light leakage at the corners of the container. The low pressures were obtained with an oil diffusion vacuum chamber utilizing a liquid nitrogen cold trap.

After the pump had been operating for approximately twenty-two hours, three initial illumination points were established as follows: the applied voltage across the lamp was adjusted until a value of detector current was reached approximating that obtained for the same detector under non-vacuum conditions when subjected to a known illumination from a tungsten filament which had a temperature of 2900°K. (The photocell was biased at 1.5 volts dc for these tests.) Two other illuminations were established similarly. The photocell currents used from the non-vacuum data were those obtained for 0.01, 0.1, and 1.0 foot-candles. As the color temperature of the optical output from the lamp in the vacuum was decidedly different from 2900°K, it is incorrect to give each illumination a definite foot-candle rating unless the filament temperature is also quoted for each point. Therefore, the data obtained for this test, Table 2, are designated as illuminations A, B, and C and are plotted in decade points in Figure 24 merely as a comparison. The straight lines between the points in Figure 24 are not intended as a suggestion of the possible variation of the current for intermediate illuminations but are used only to group corresponding sets of points.

Approximately twenty-four hours after the initial points were established, the first observation was made. At this time, a dark current value was measured. Then, the same precise bias voltages were applied to the lamp as used for the above illuminations and the resulting currents recorded. Two more observations were made at the end of approximately twenty-four hour intervals. During these intervals, the photocell was biased at 1.5 volts dc in the dark. Near the end of the third twenty-four-hour period, a small tear was discovered in the aluminum foil near one corner of the container. By shining a light directly on the tear, a small fluctuation on the picoammeter was observed. This explains why the "dark" detector currents recorded during the vacuum environment test (Table 2) are so much larger than the corresponding values (Table 3) obtained for photocell current versus illumination tests conducted before and after the vacuum environment test. The data shown in Table 3 are plotted in Figure 24.

Table 2. Vacuum Environment Test Data

Observation	Hours Elapsed Since Last Observation	Pressure (torr)	Photocell Current Values for a Lamp Bias of			
			0V("dark")	1.050000V	1.435000V	2.095000V
Initial	---	5×10^{-6}	2.16×10^{-9}	7.45×10^{-6}	8.13×10^{-5}	5.25×10^{-4}
1st	25 1/3	7×10^{-6}	2.50×10^{-9}	1.08×10^{-5}	9.4×10^{-5}	5.30×10^{-4}
2nd	26 1/6	6×10^{-6}	3.30×10^{-9}	1.16×10^{-5}	1.00×10^{-4}	5.45×10^{-4}
3rd	24 1/2	5×10^{-6}	3.25×10^{-9}	1.15×10^{-5}	1.00×10^{-4}	5.45×10^{-4}

From the data recorded, it appeared that no further information could be obtained for this setup, and the test was discontinued after the third observation. The cause for the apparent variations shown in Figure 24 is probably not due to "ageing" of the photocell as it was heat cycled before the test. It could be the result of a small change of the lamp characteristics due to outgassing of the filament during the test.

Table 3. Photocell Current Versus Illumination
Data Taken Before and After Vacuum Environment Test

	Photocell Current (in amps)					
	Dark	10^{-4} ft-c	10^{-2} ft-c	1 ft-c	10^{2} ft-c	10^{4} ft-c
Before	1.5×10^{-11}	4.5×10^{-11}	8.8×10^{-8}	8.0×10^{-5}	2.95×10^{-3}	2.5×10^{-2}
After	1.5×10^{-11}	5.0×10^{-11}	8.4×10^{-8}	8.5×10^{-5}	3.0×10^{-3}	2.5×10^{-2}

The conclusion drawn from this section of the evaluation is that a vacuum environment does not affect the operating characteristics of the detectors.

8. LIGHT MEMORY EFFECTS

In an attempt to evaluate the effects of prolonged storage of thin film CdS photodetectors in either the light or dark, the following experiment was conducted. Two detectors were selected. One of the units was placed in the dark and the second was left exposed to room light (approximately 10 foot-candles) for a period of 66 hours. Upon removal of the detectors from their storage environment, a photocurrent versus illumination curve was measured in the following manner: The unit which was stored in the dark was maintained in the dark until the beginning of the measurement. The photocurrent versus illumination curve was taken by starting from the dark and increasing the light level while monitoring the current as a function of the light level. The unit which was stored in room light was maintained in room light and the same curve taken with decreasing illumination. Figure 25 is a plot of the photocurrent-illumination characteristics of the two detectors prior to storage. Figure 26 is the same measurement after storage and measured as described above. Inspection of the two figures indicates only very slight differences in the characteristics due to this storage. These small differences are probably within the experimental error of the test.

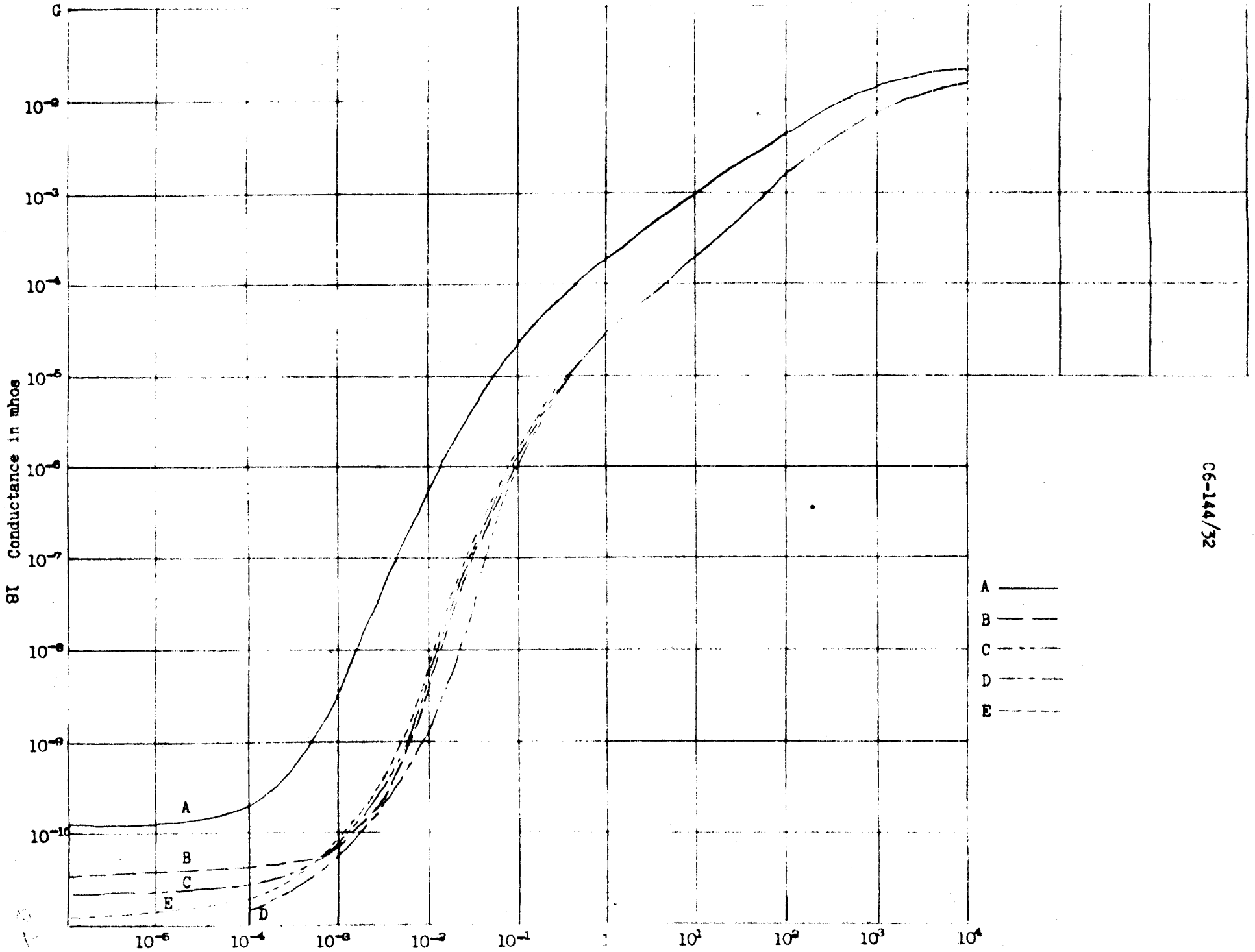

Figure 1. Illumination in Ft-Candles Detector JPL-20 Over Four Sterilization Cycles

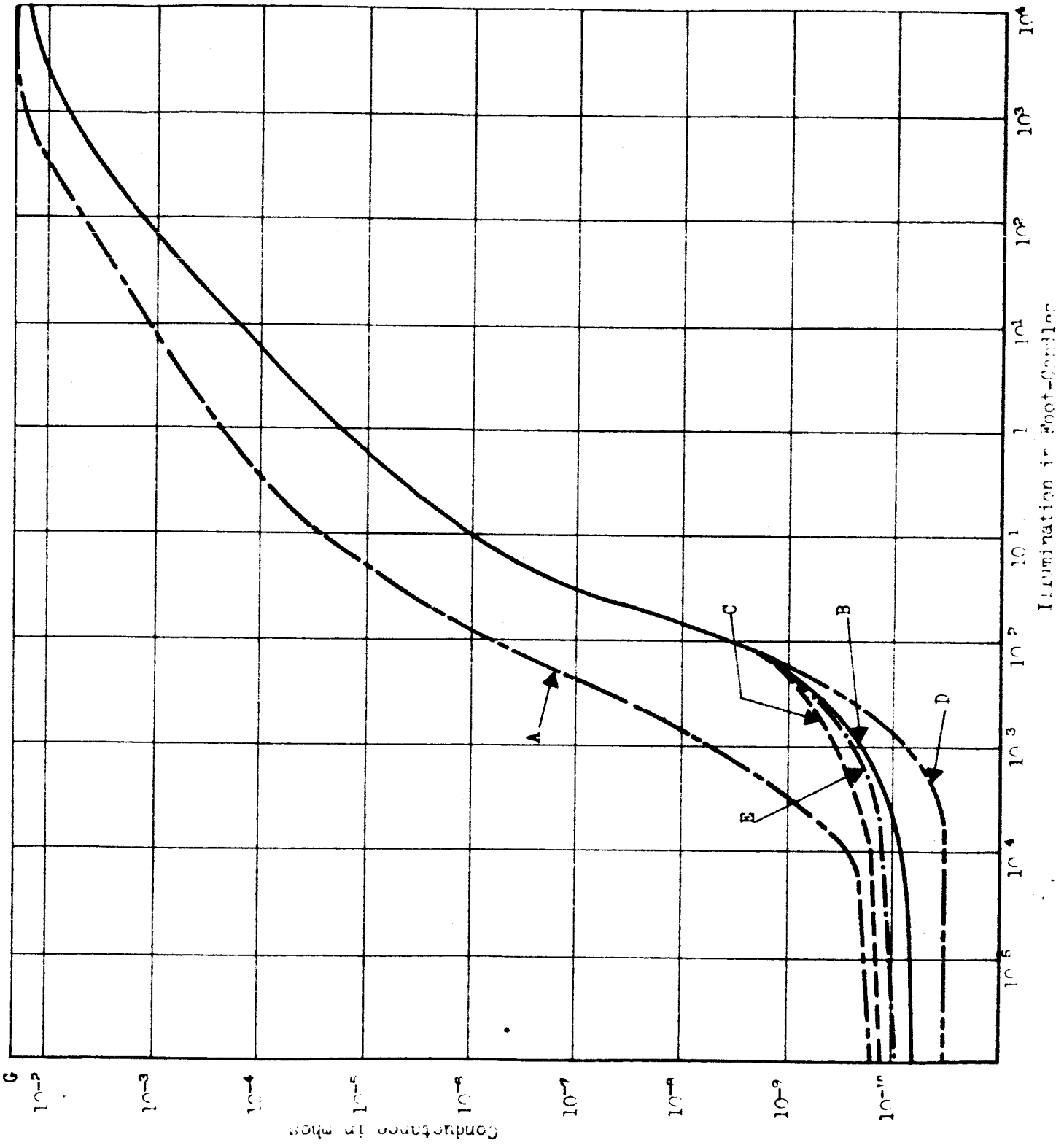

Figure 2.
Detector JPL-21 Over Four Sterilization Cycles

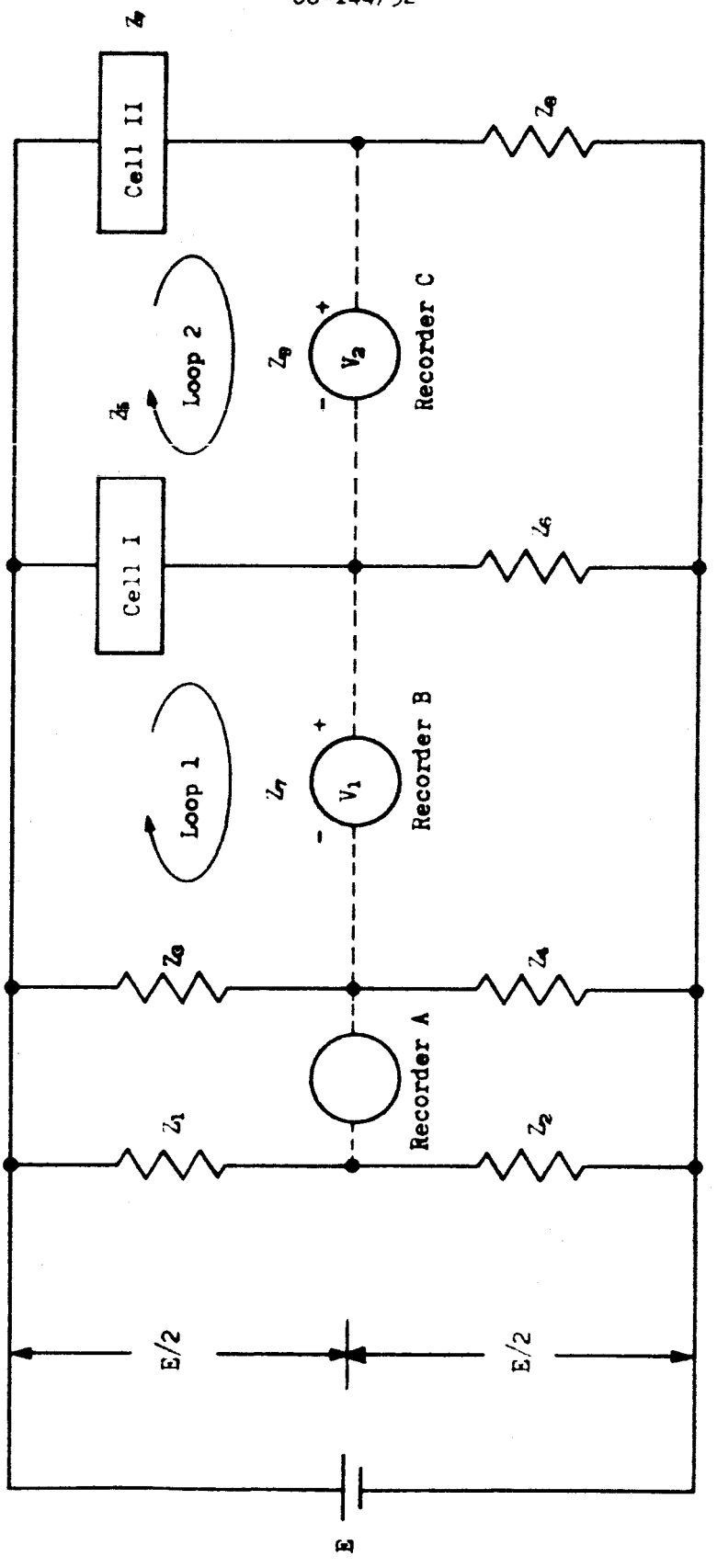

Figure 3. Bridge Circuit

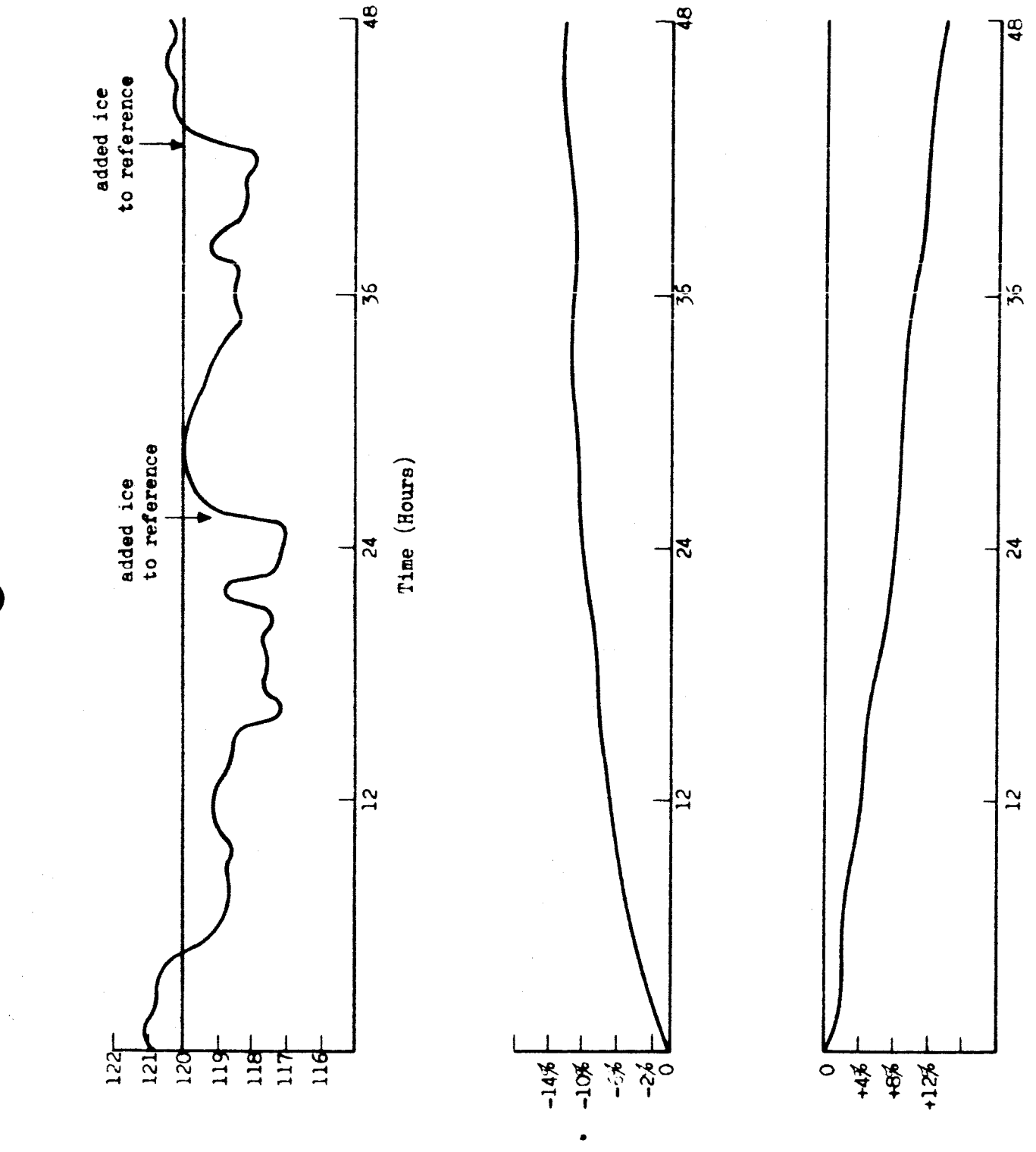

Figure 4. Long Term Null Stability

Illumination: 1 ft-c
Temperature: 120°F

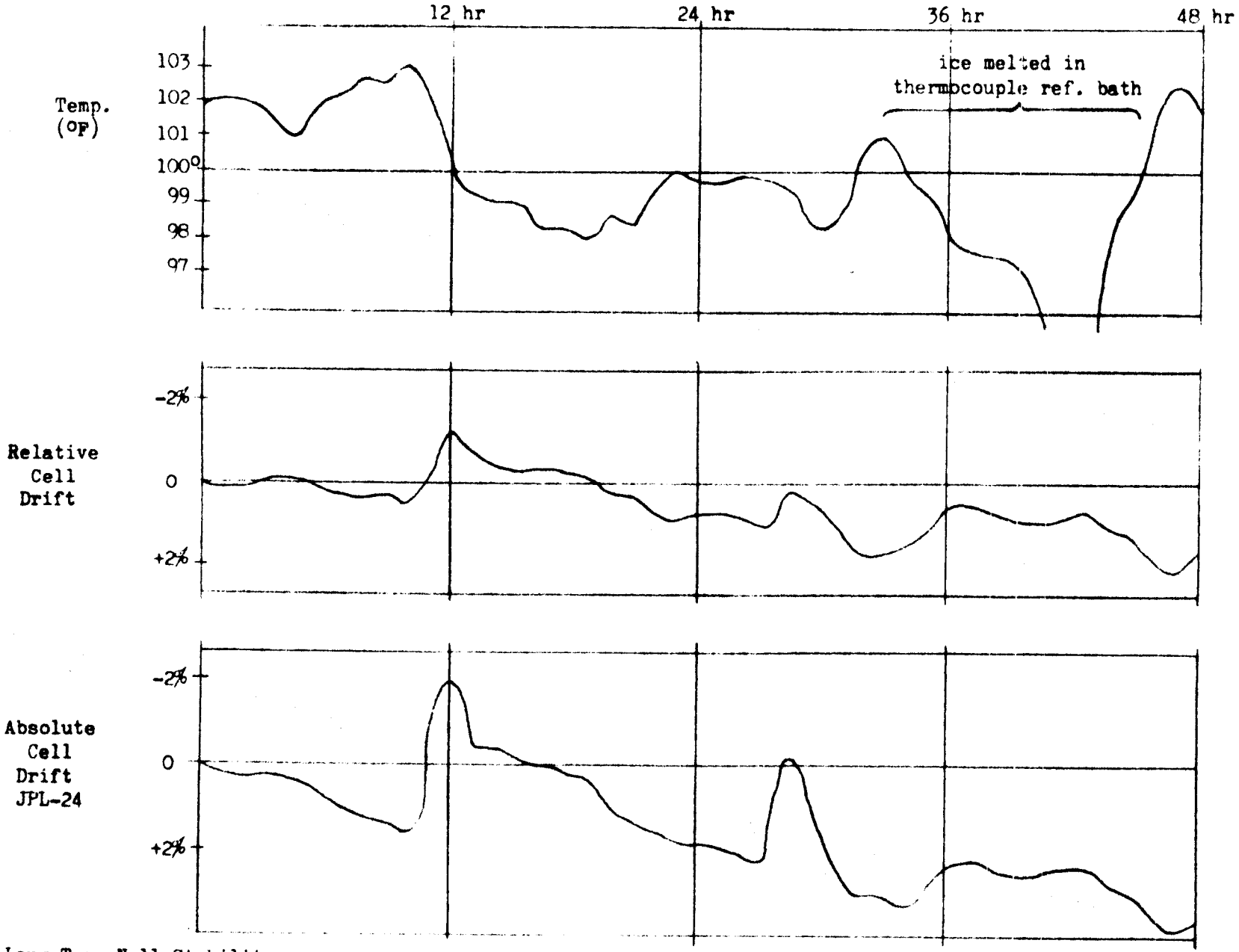

Long Term Null Stability
Temperature: 100°F
Illumination: 1 ft-candle

Figure 5

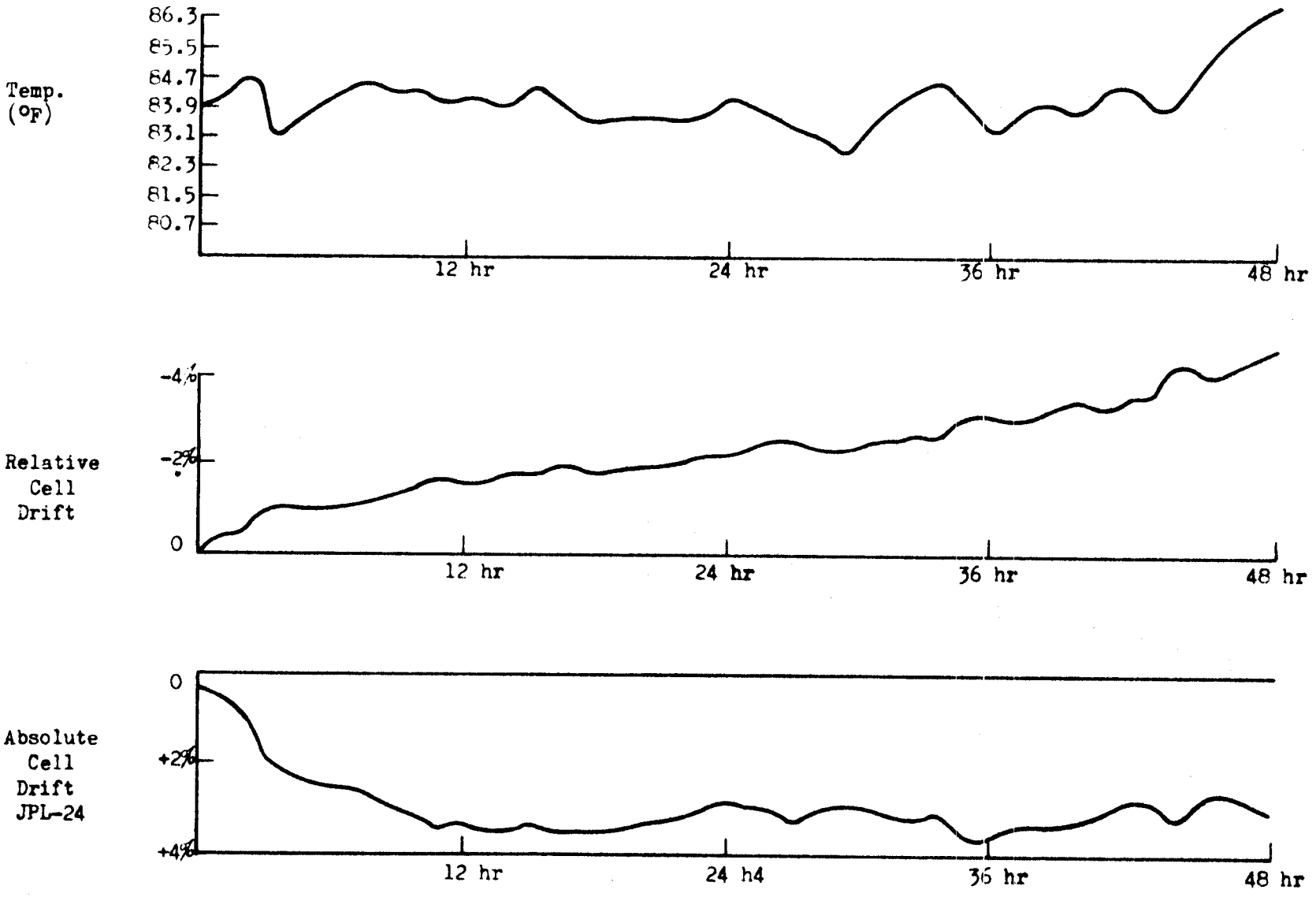

Temperature: 80°F
Illumination: 1 ft-c

Figure 6. Long Term Null Stability

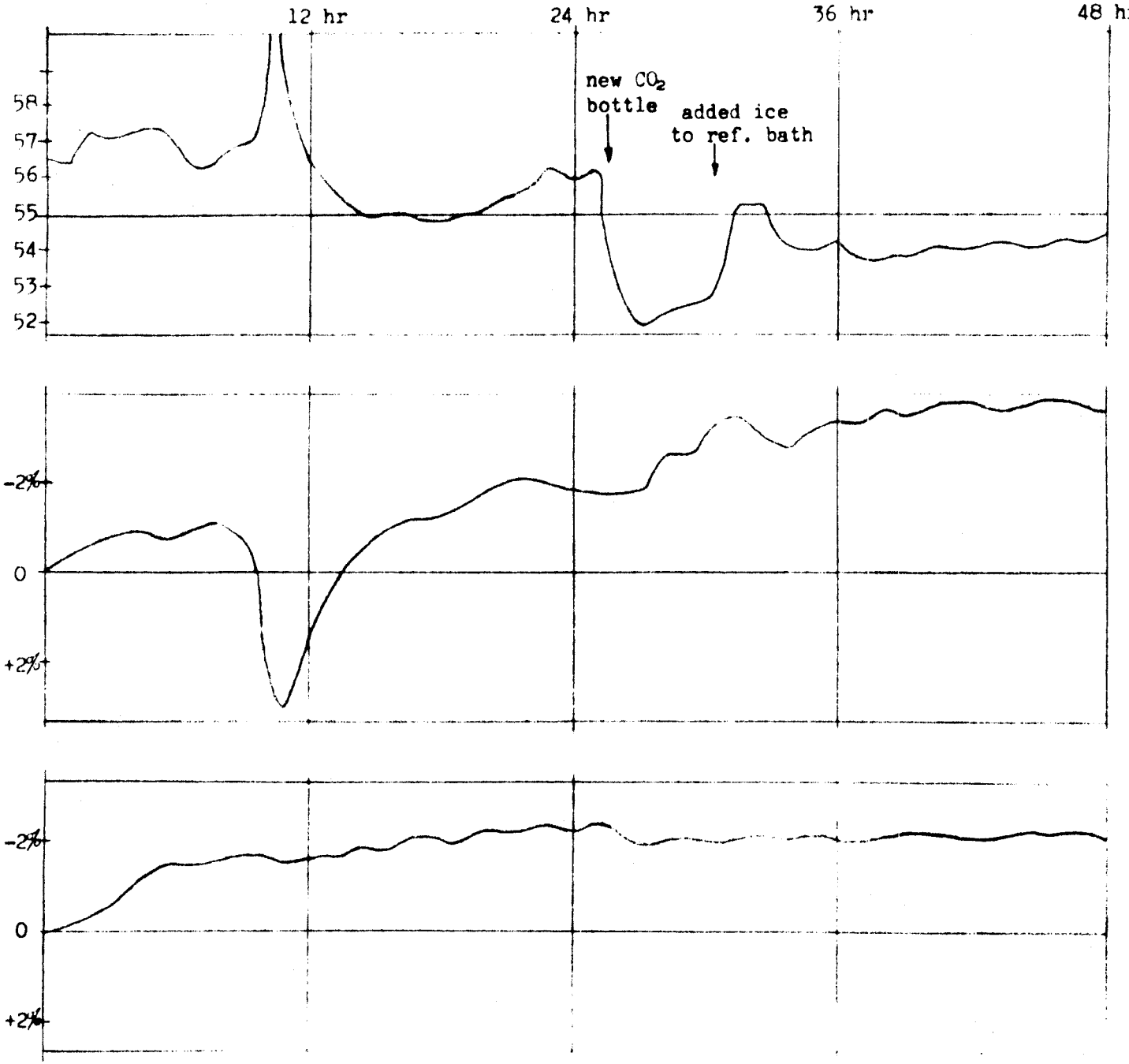

Long Term Null Stability
Temperature: 55°F
Illumination: 1 ft-candle

Figure 7

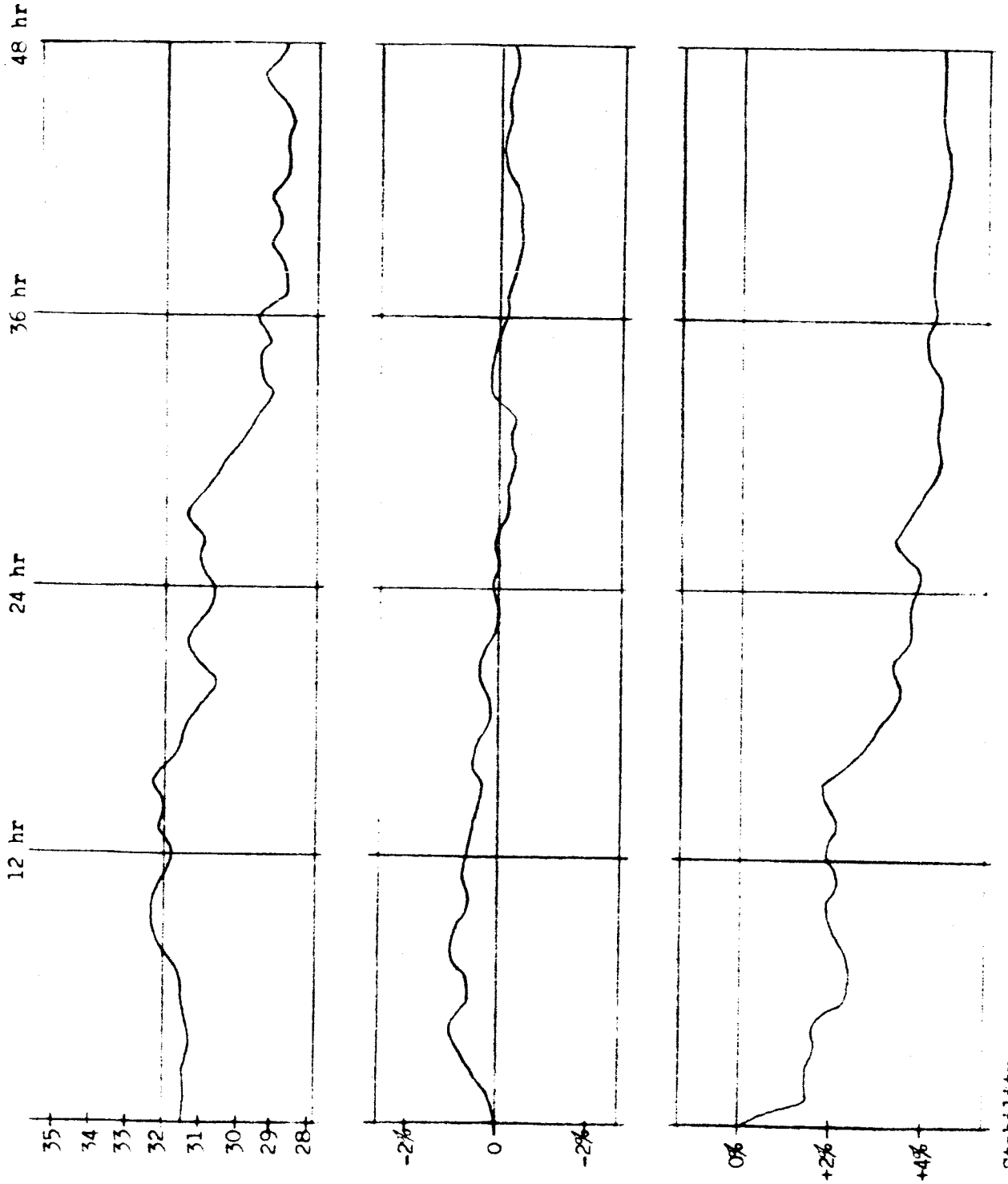

Long Term Null Stability
Temperature: 32°F
Illumination: 1 ft-candle

Figure 8

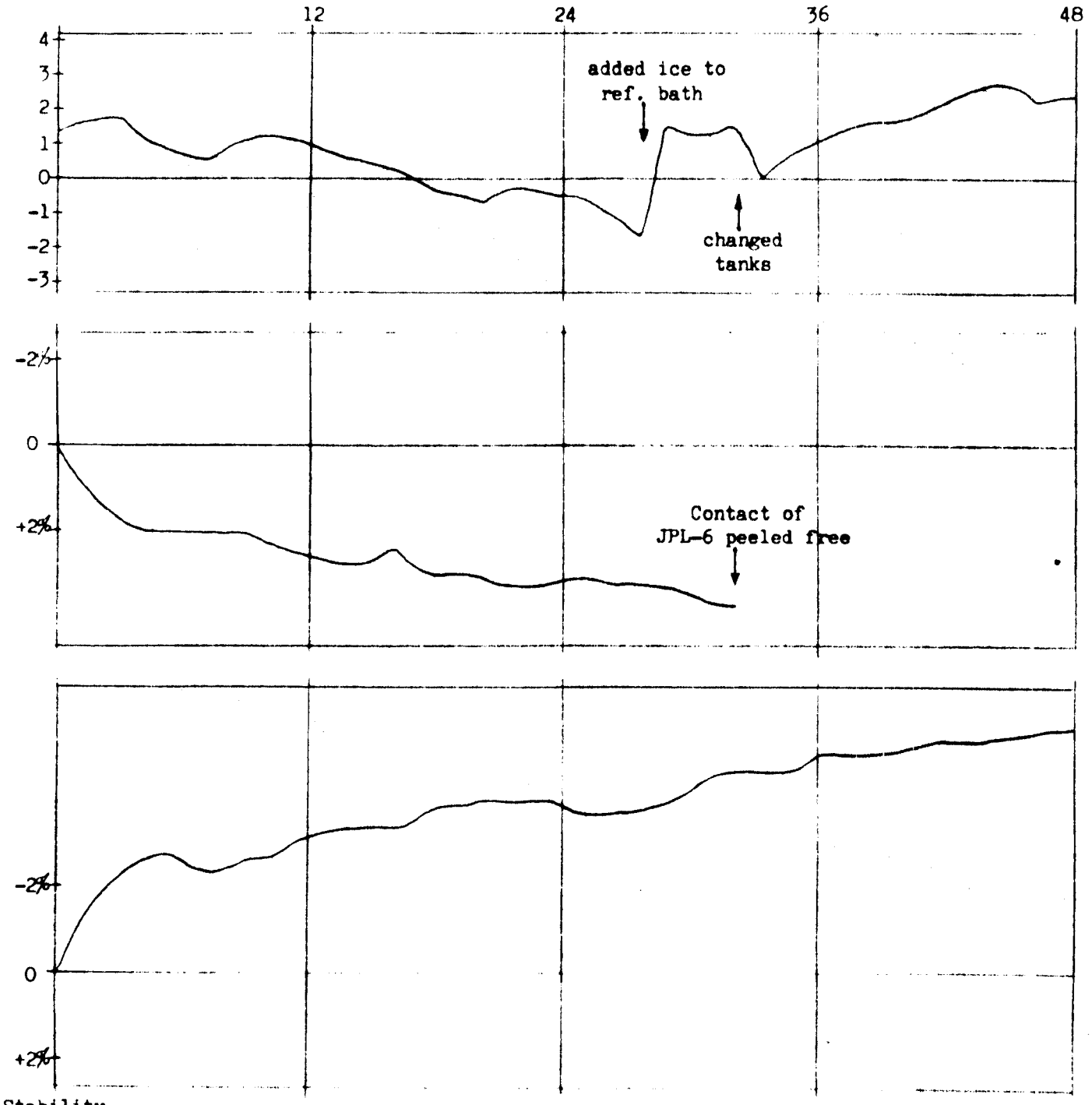

Long Term Null Stability
Temperature: 0°F
Illumination: 1 ft-candle

Figure 9

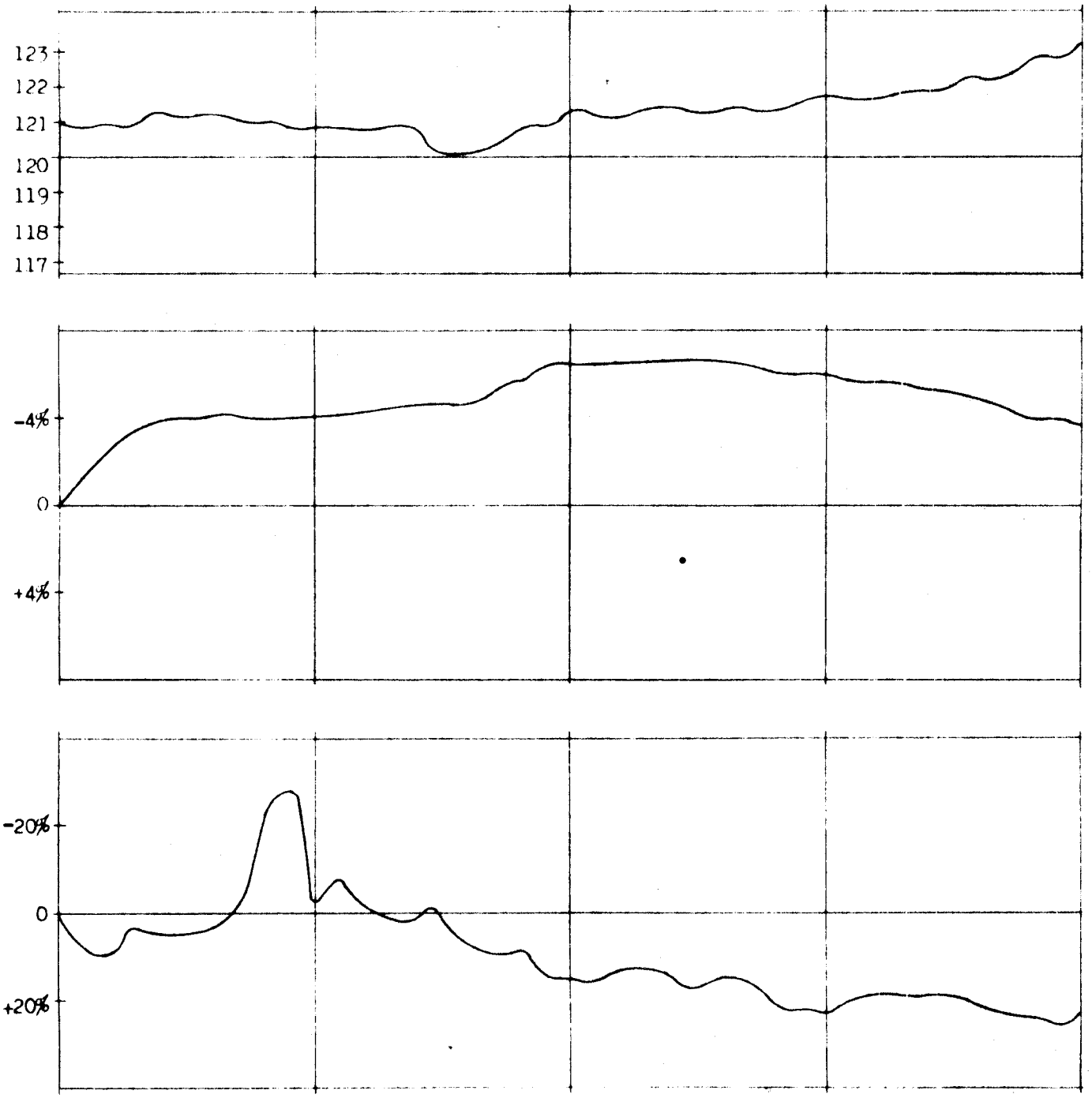

Long Term Null Stability
Temperature: 120° F
Illumination: 0.01 ft-candle

Figure 10

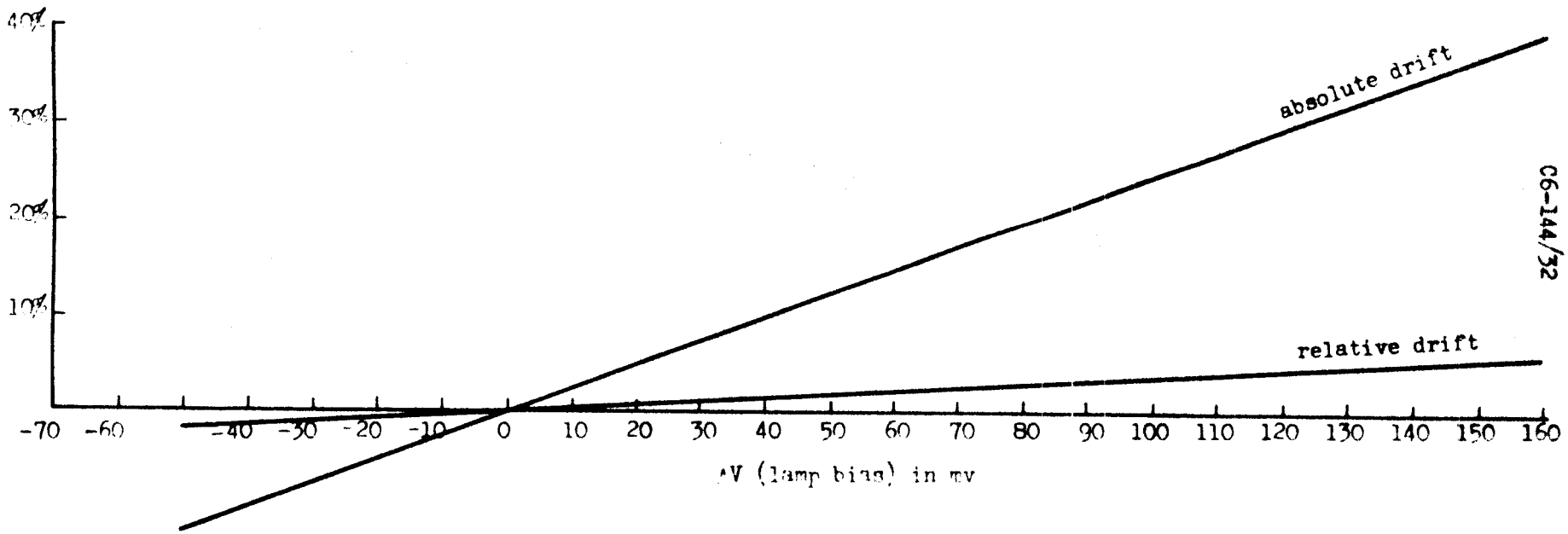

Figure 11. Drift Due to Small Change in Lamp Bias

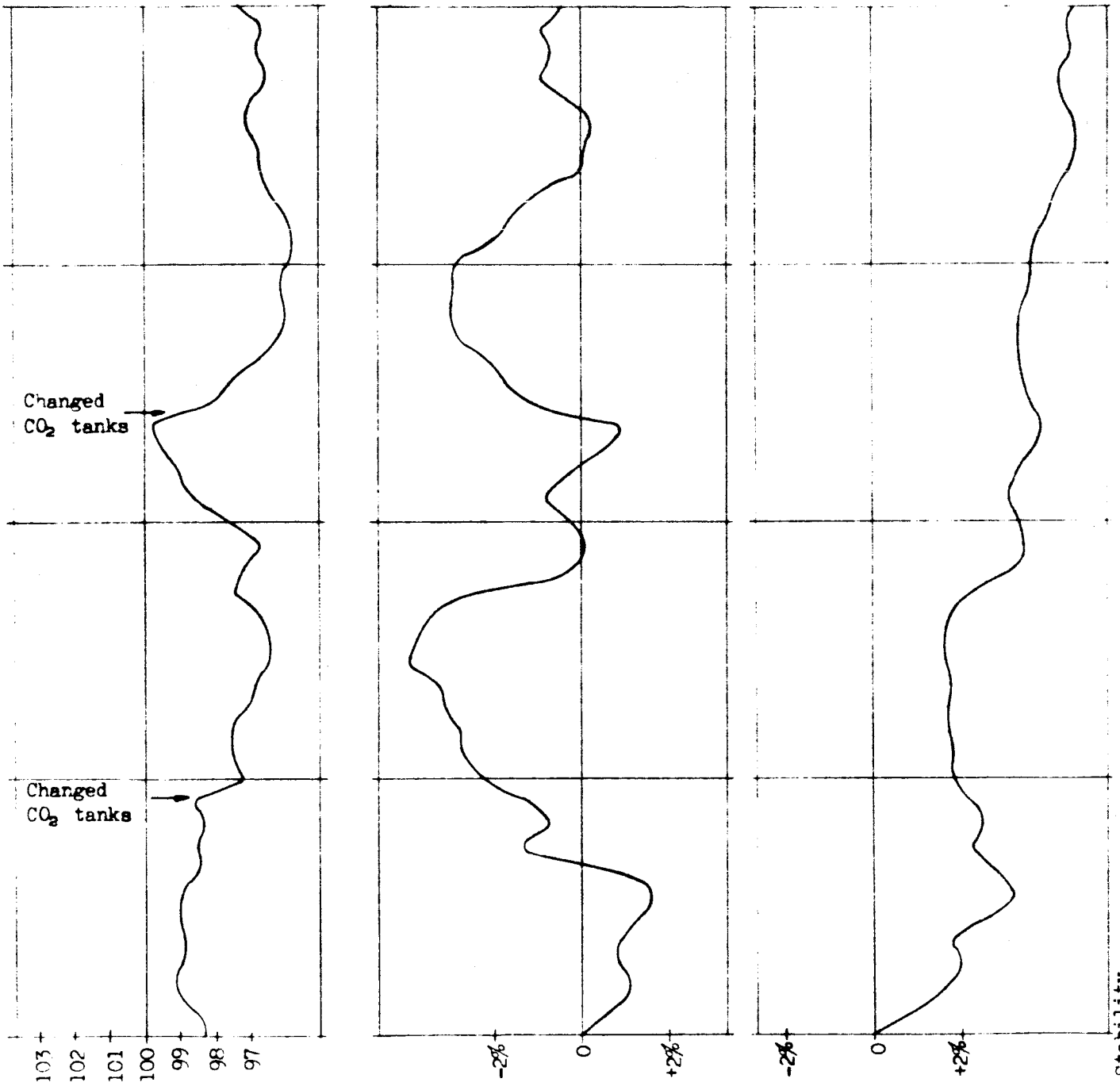

Long Term Null Stability
Temperature: 100°F
Illumination: 0.01 ft-candle

Figure 12.

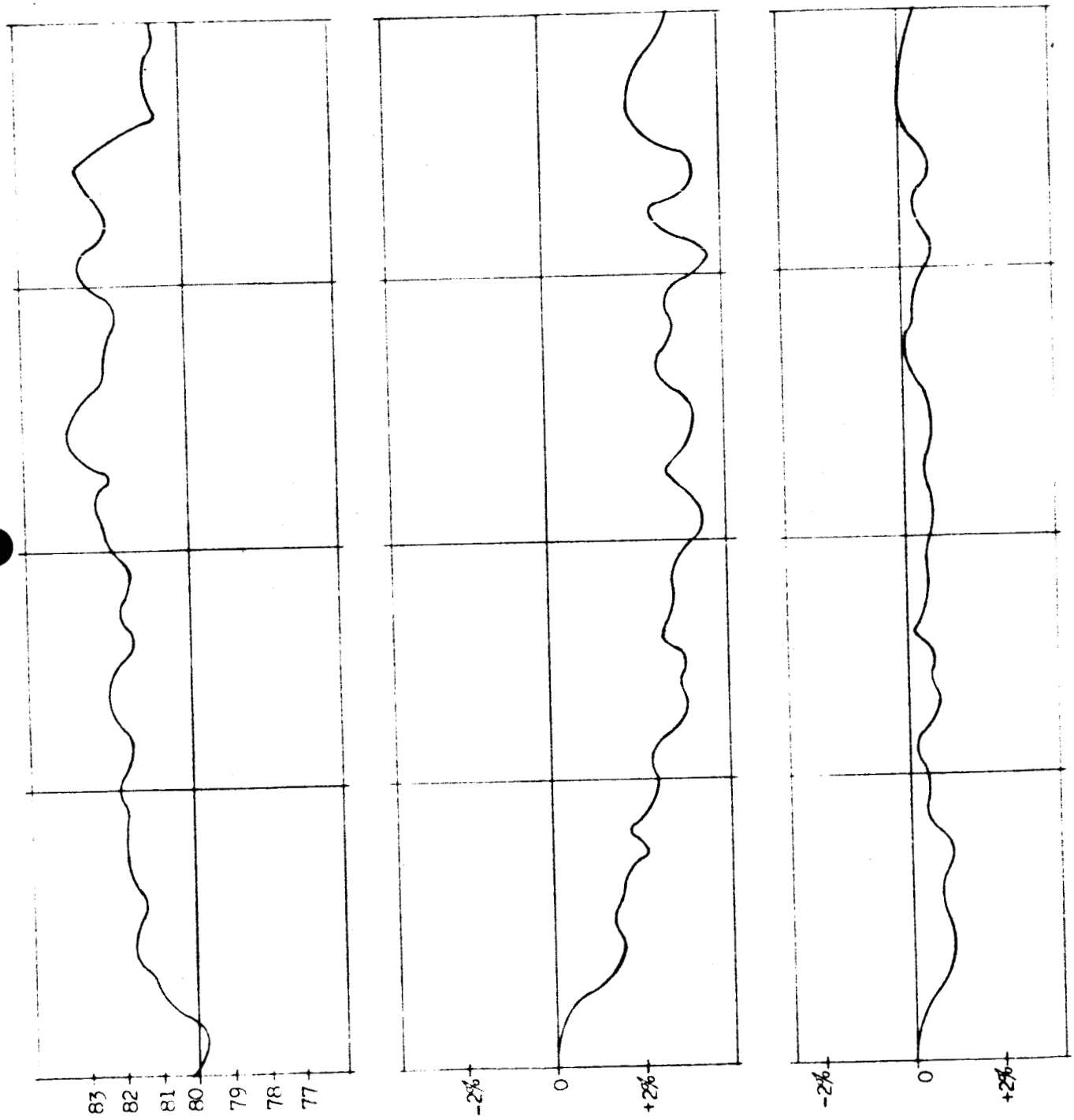

Figure 13

Long Term Null Stability
Temperature: 80° F
Illumination: 0.01 ft-candle

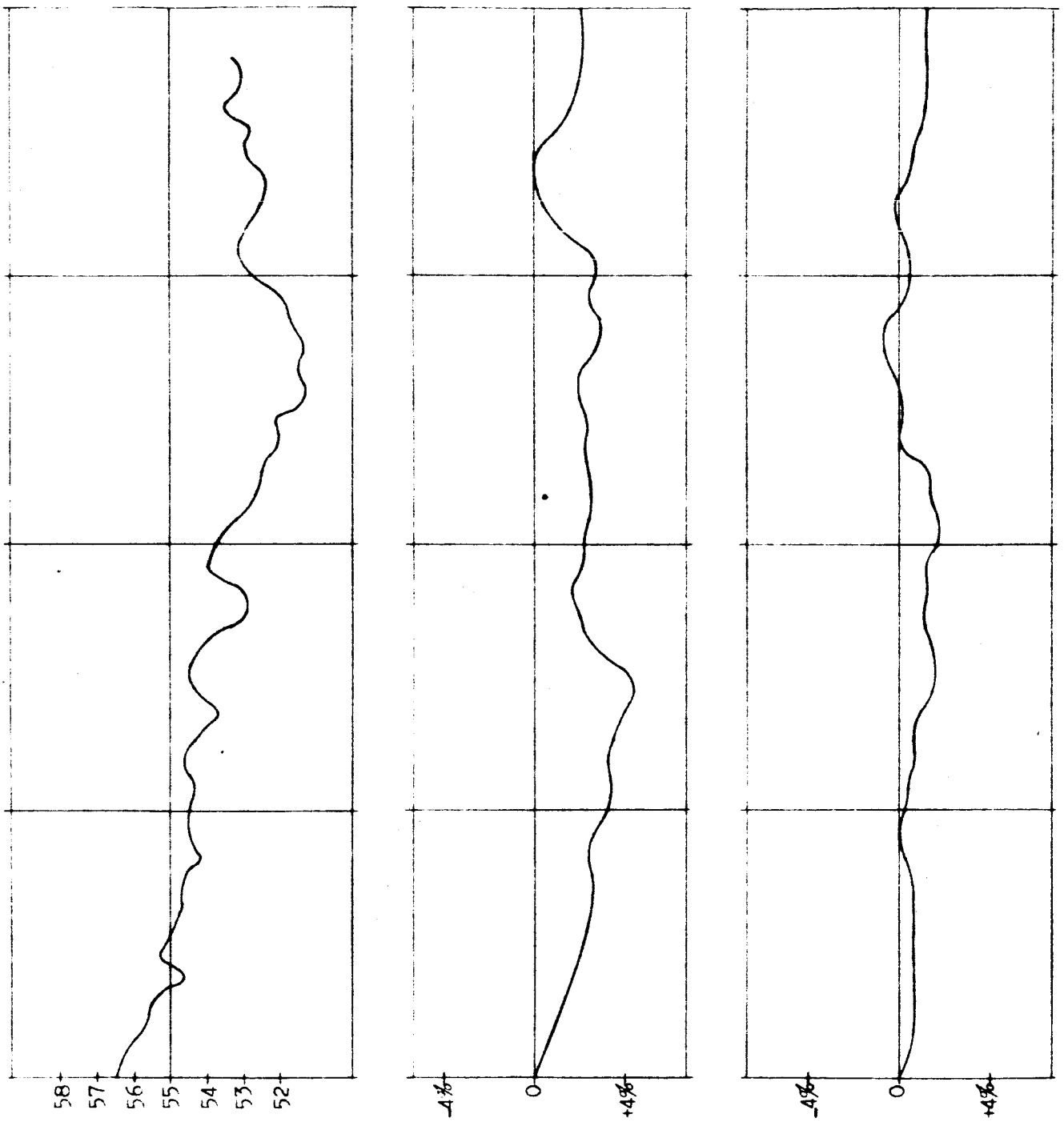

Figure 14

Long Term Null Stability
Temperature: 55° F
Illumination: 0.01 ft-candle

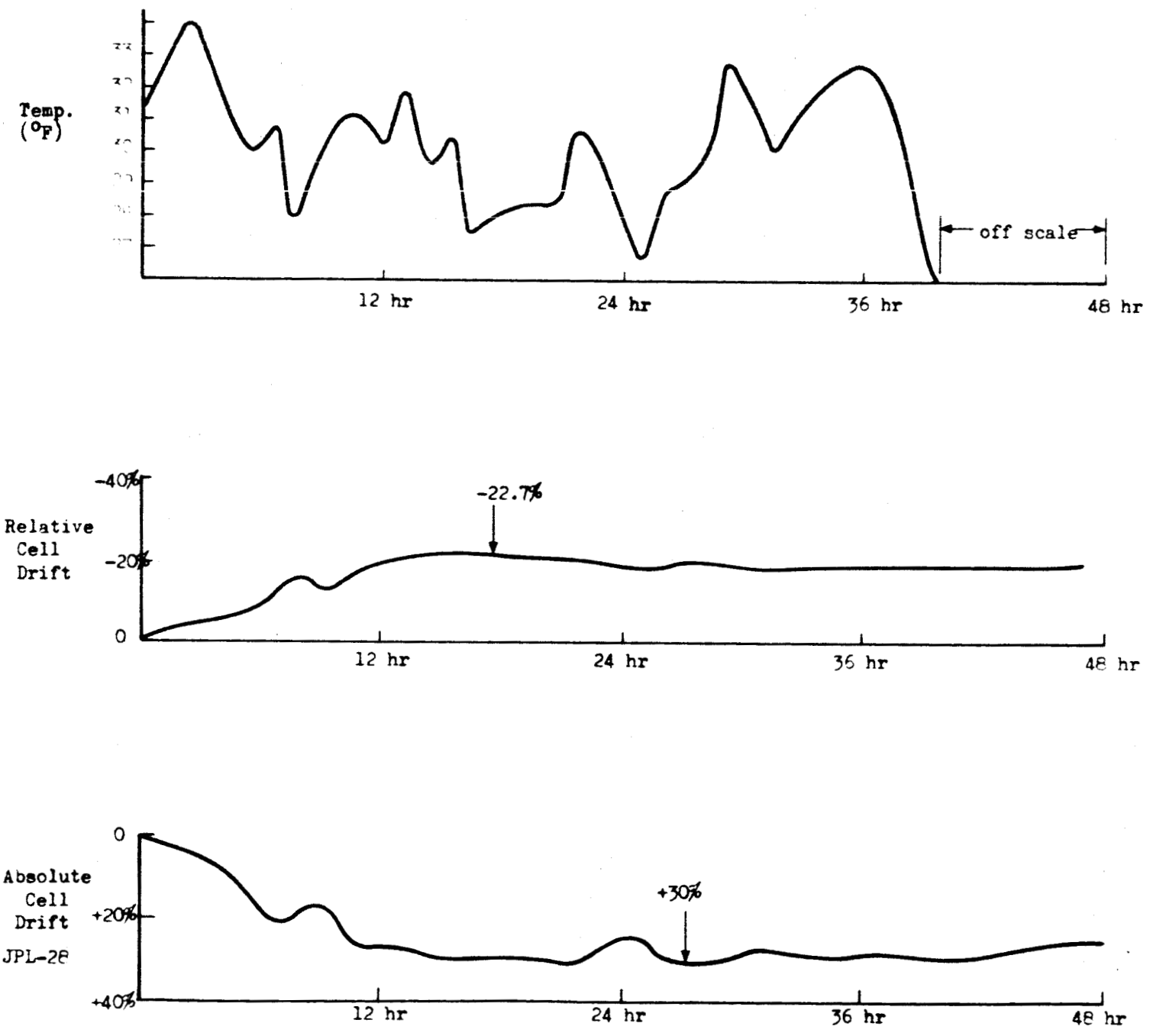

Figure 15. Long Term Null Stability

Temperature: 30°F
Illumination: 0.01 ft-c

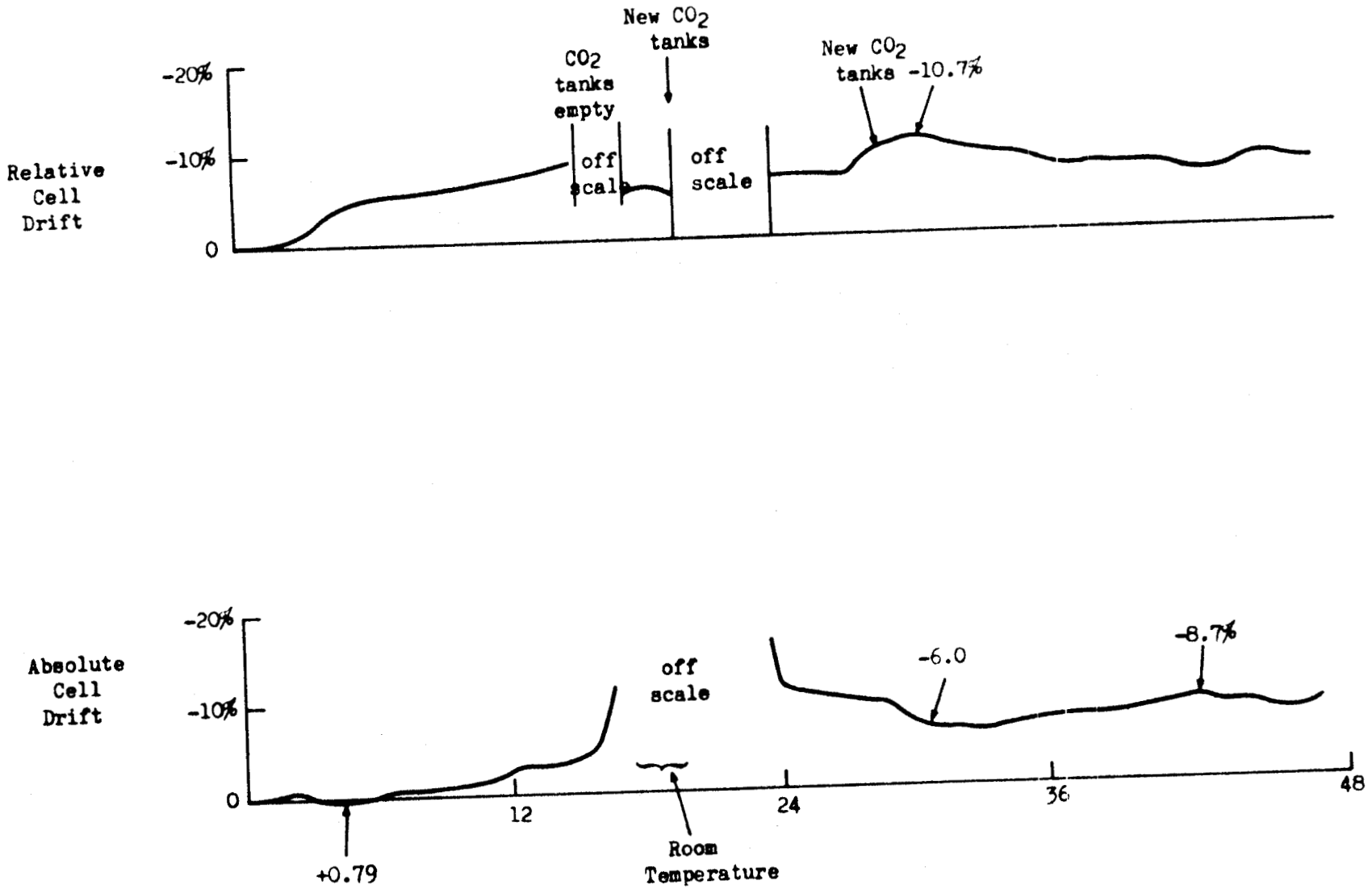

Figure 16. Long Term Null Stability

Temperature: -14°F
Illumination: 0.01 ft-c

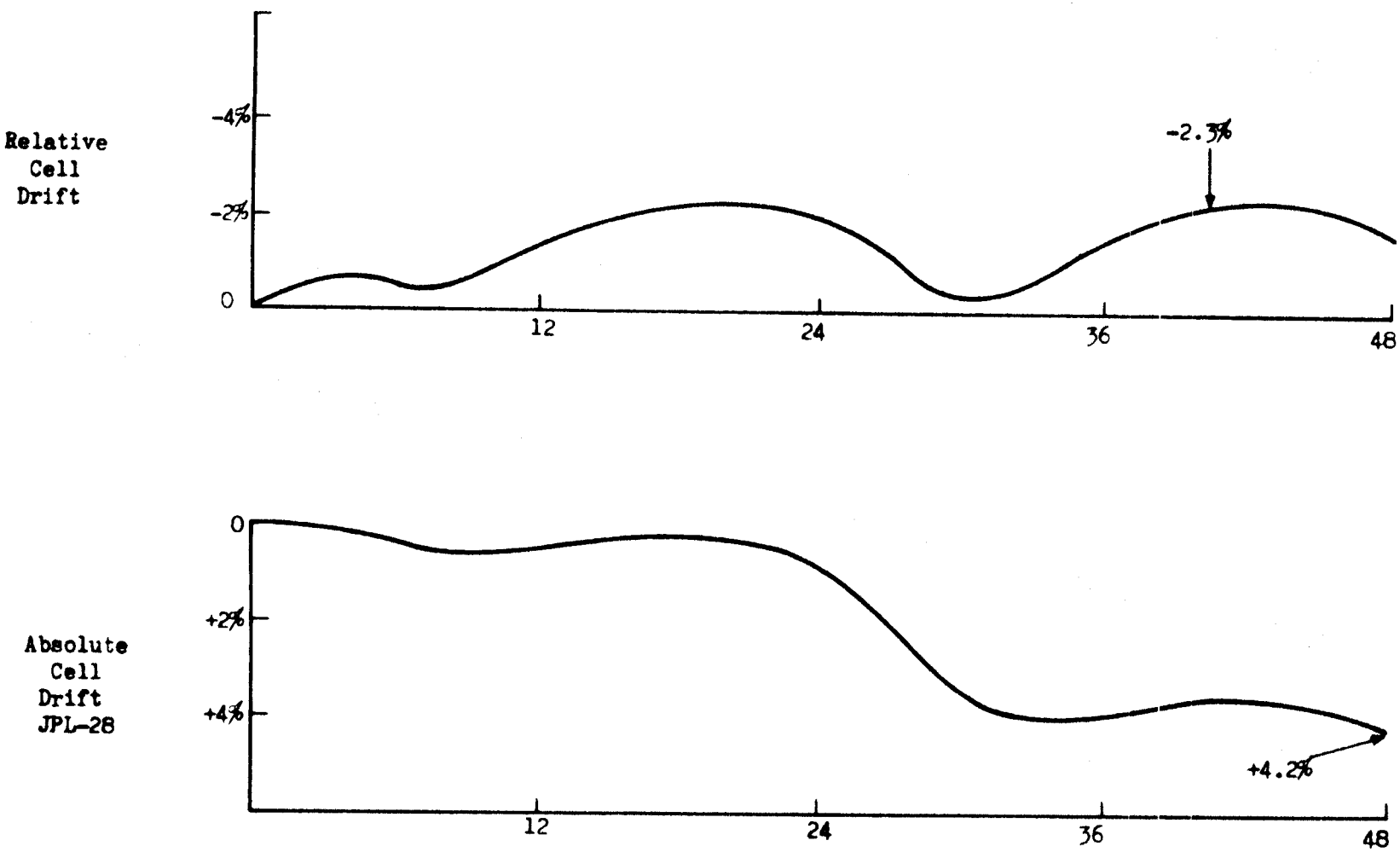

Temperature: 120° ± 1°F
Illumination: 100 ft-c

Figure 17. Long Term Null Stability

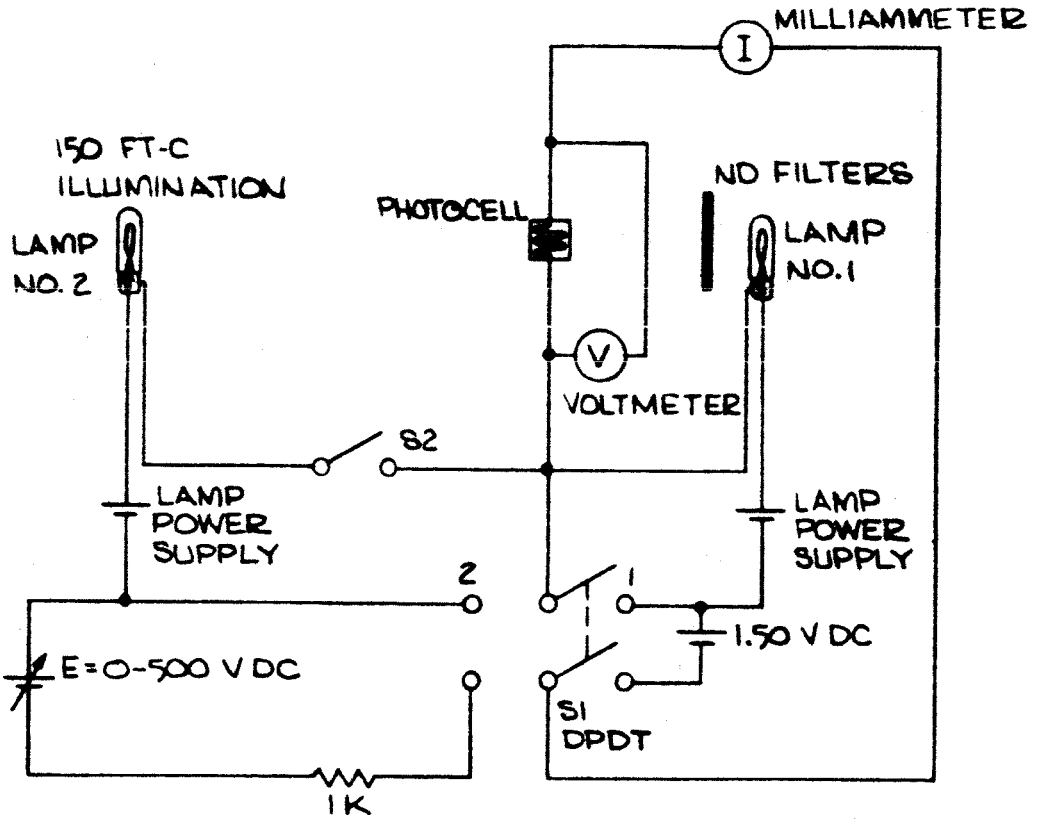

TEST CIRCUIT FOR MAXIMUM OPERATING LIMITS

FIGURE 18

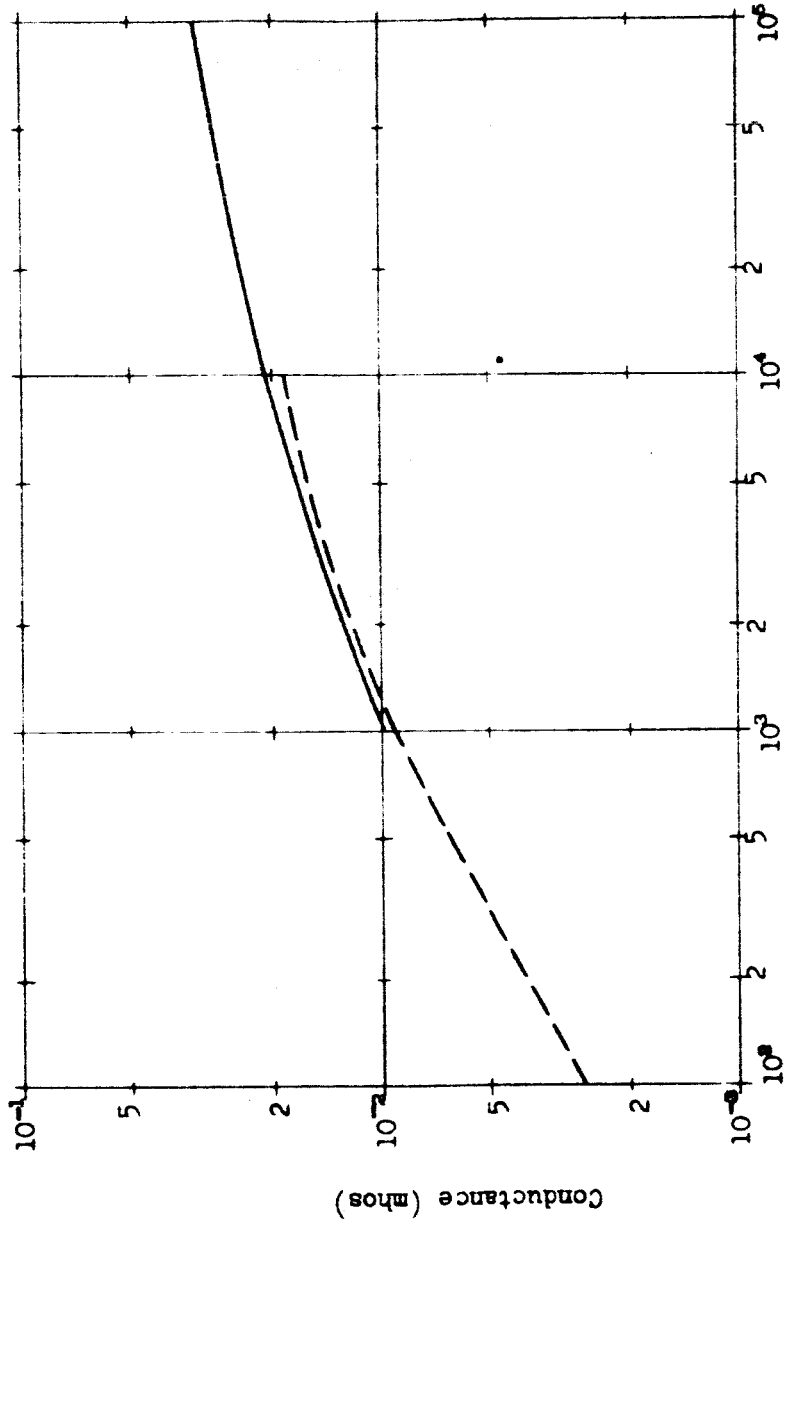

Figure 19

High Illumination Tests

	0.01	0.1	1
0.01	A	B	C
0.1	D	E	F
1		G	H

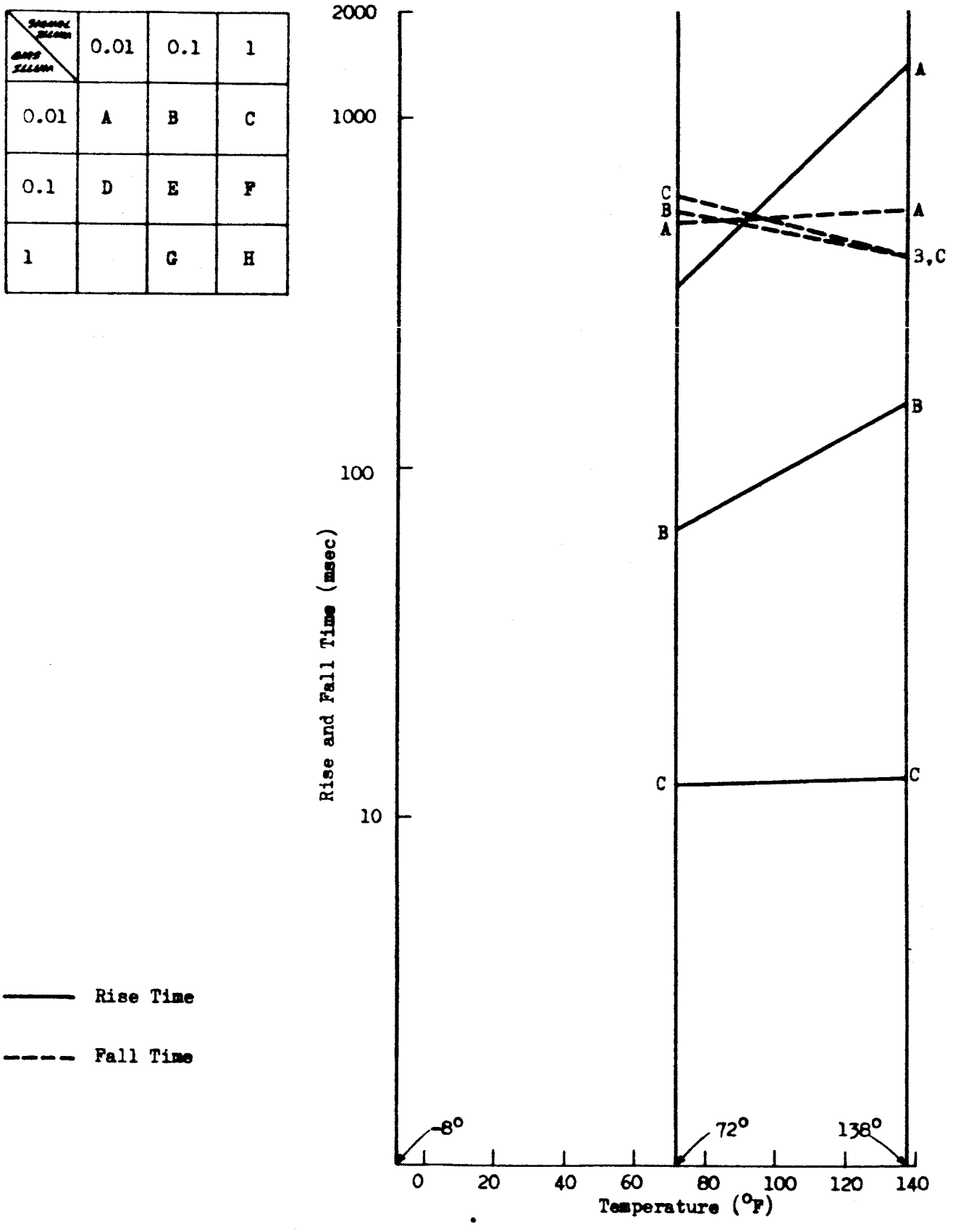

Figure 20. Rise and Fall Times versus Temperature

Signal Illum / Bias Illum	0.01	0.1	1
0.01	A	B	C
0.1	D	E	F
1		G	H

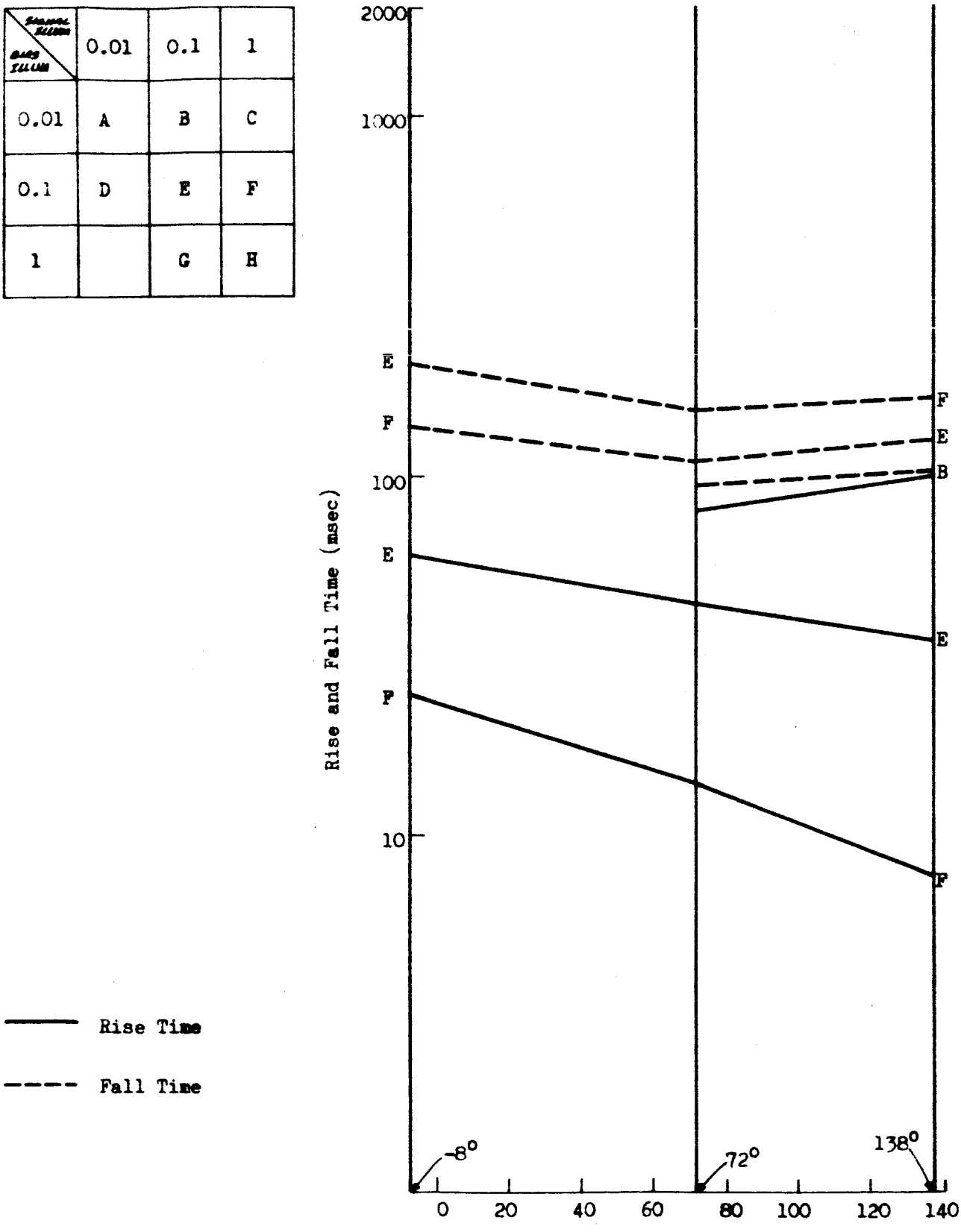

Figure 21. Rise and Fall Times vs Temperature

	0.01	0.1	1
0.01	A	B	C
0.1	D	E	F
1		G	H

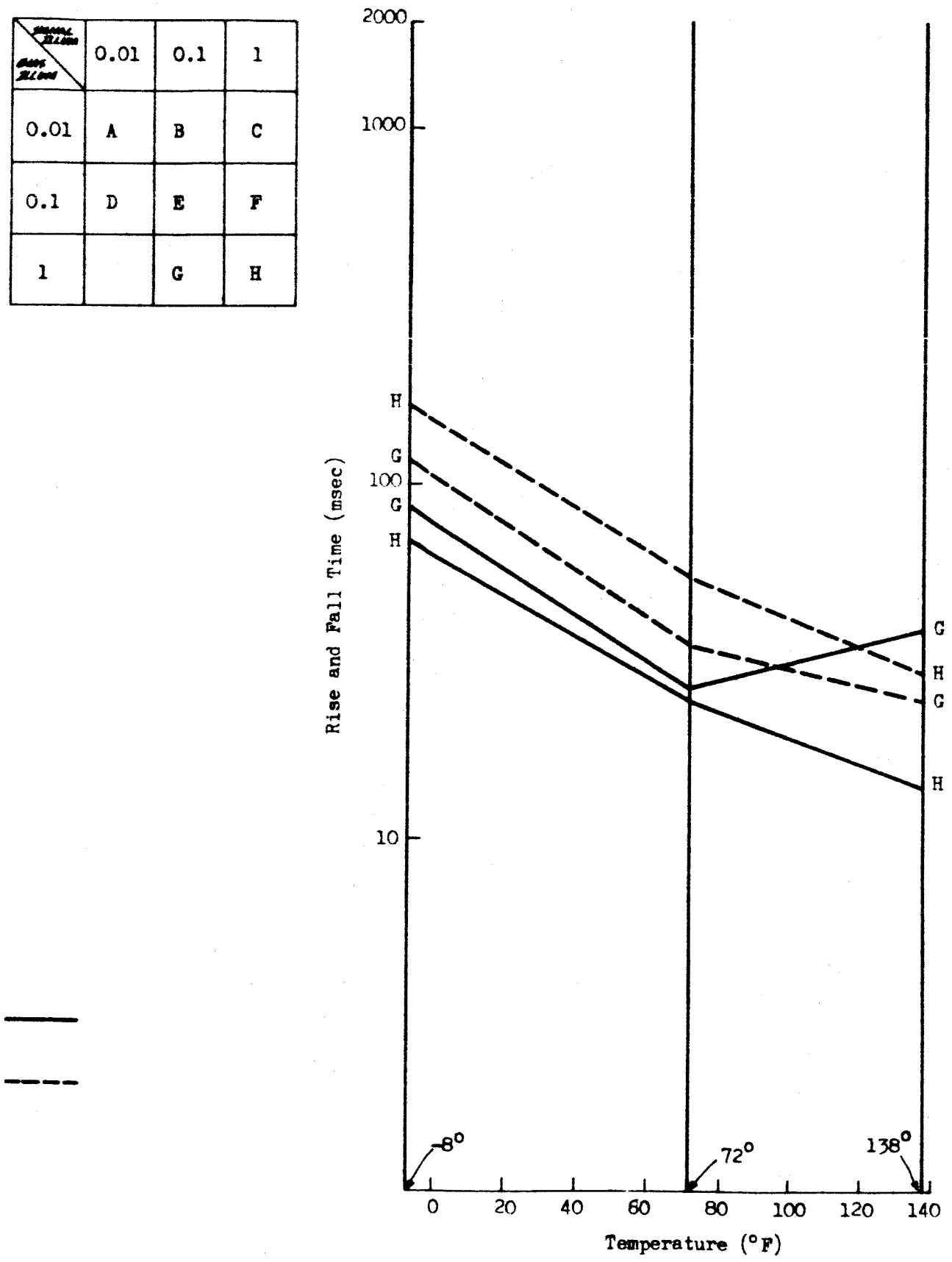

Figure 22. Rise and Fall Times versus Temperature

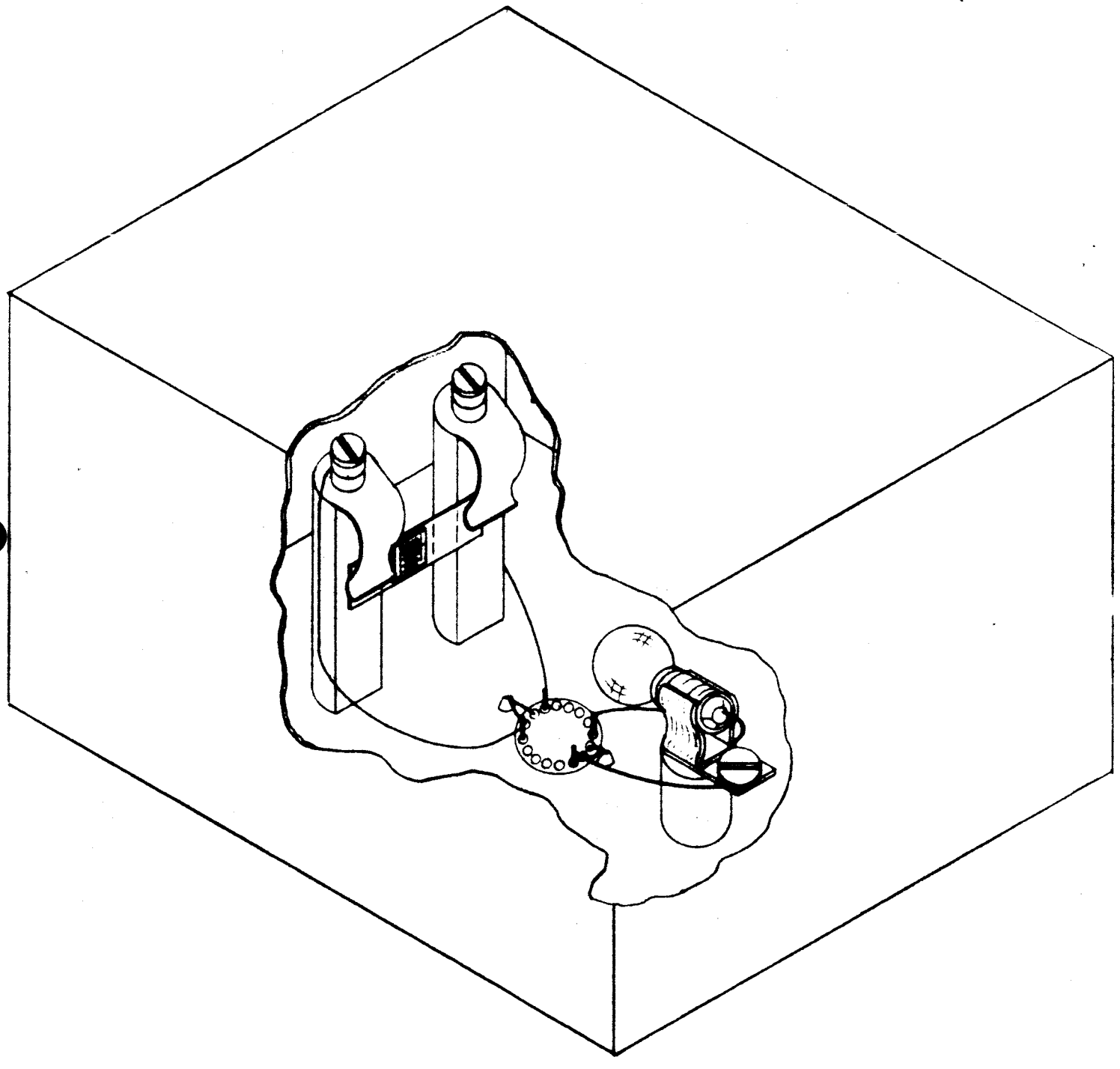

TEST SETUP FOR VACUUM ENVIRONMENT TEST

FIGURE 23

LEGEND: C6-144/32

——— INITIAL OBSERVATION

- - - - - 1ST OBSERVATION

——— 2ND & 3RD OBSERVATION

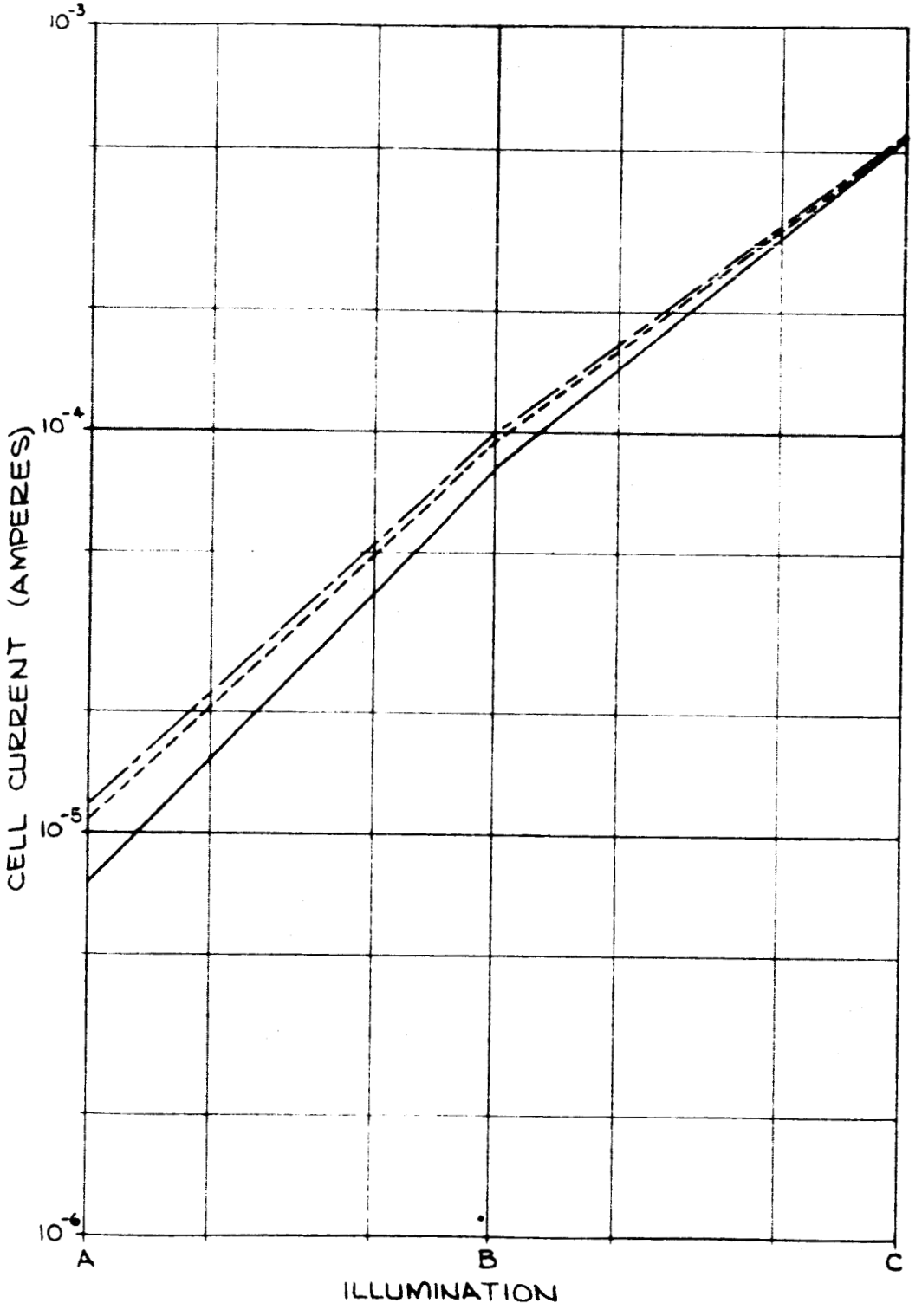

VACUUM ENVIRONMENT TEST DATA

FIGURE 24

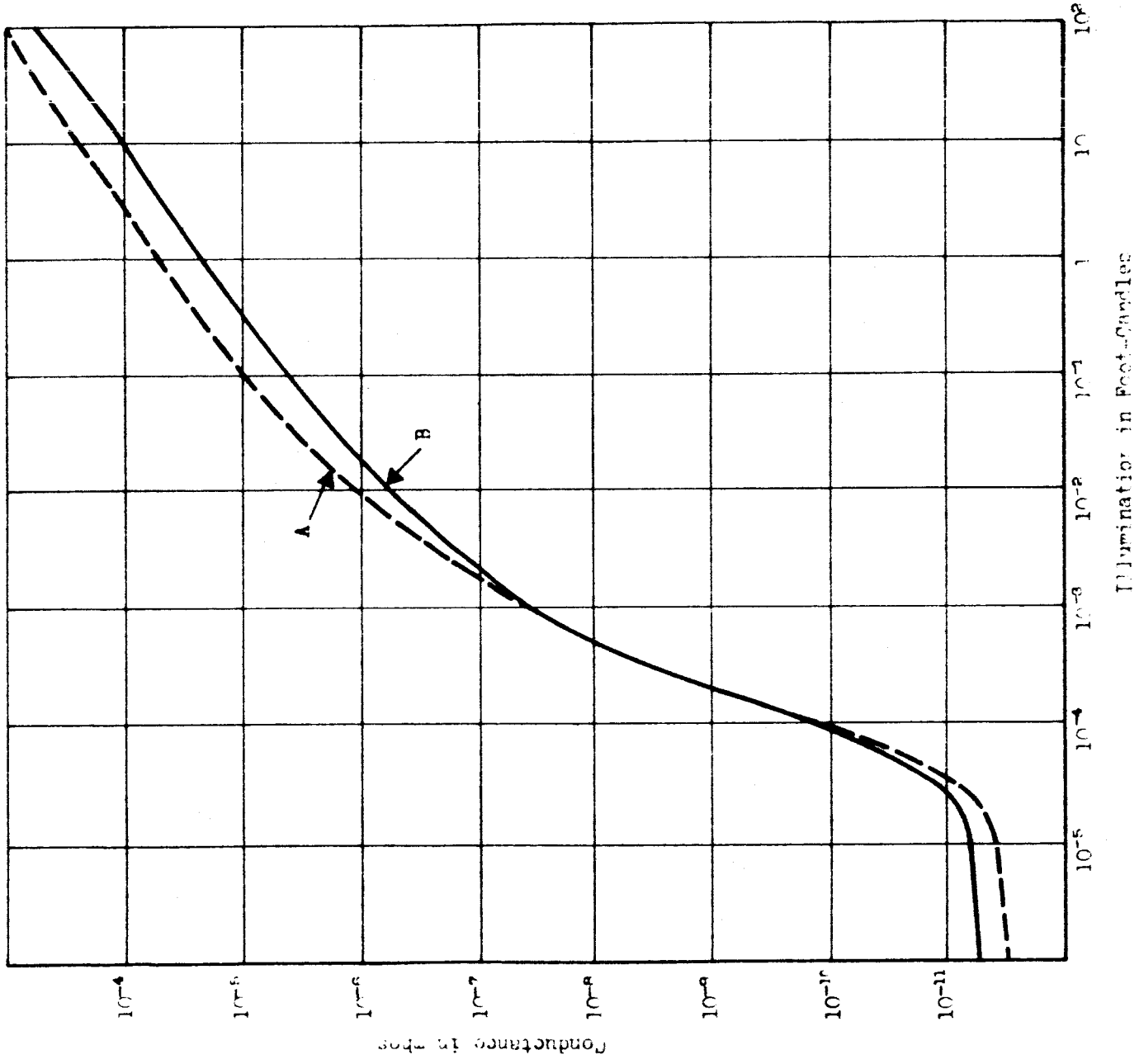

Figure 25. Light Memory Effects **Before Storage**

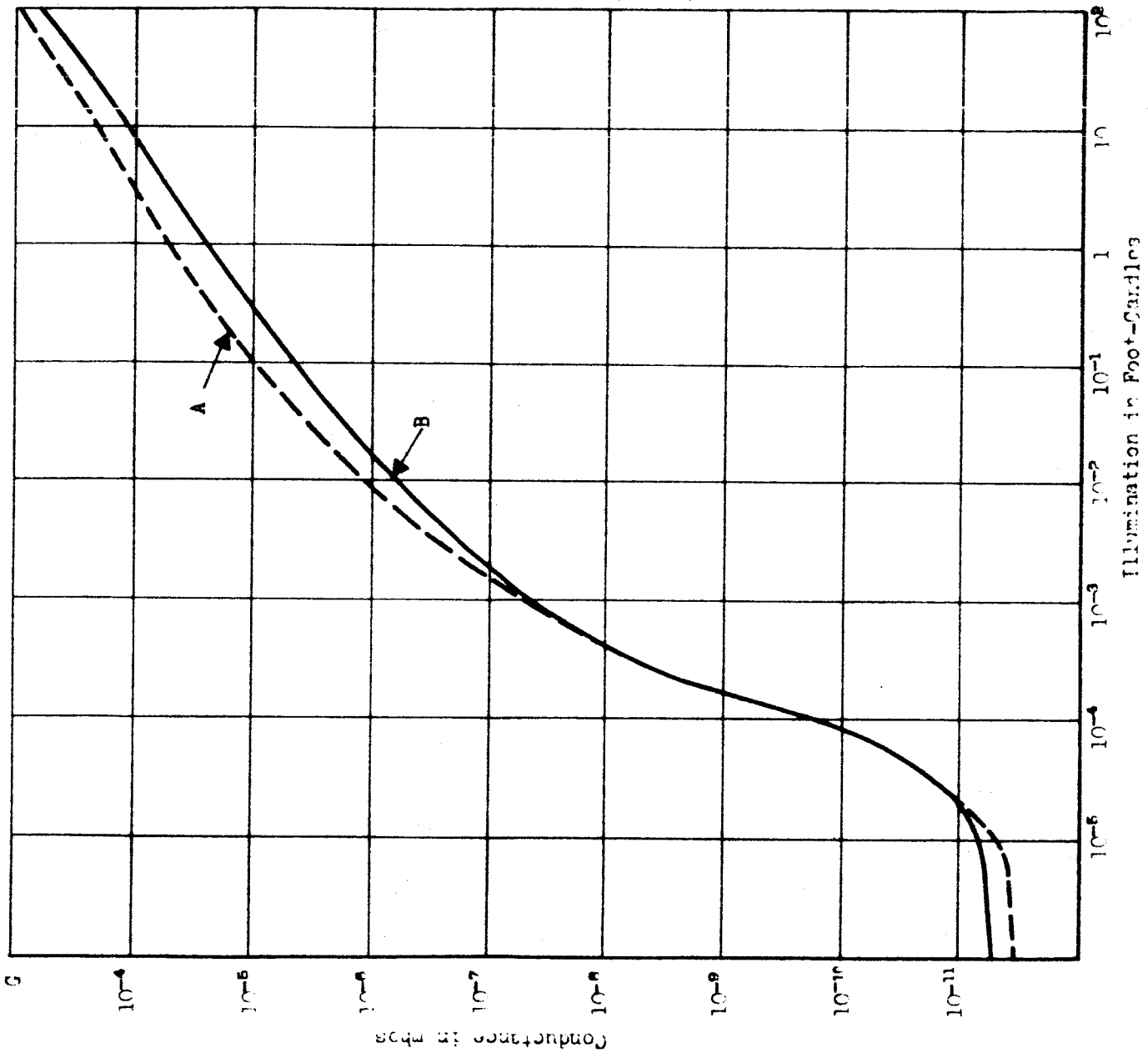

Figure 24. Light Memory Effects After Storage

APPENDIX

The null stability between two matched photocells has been determined as follows. Shown in Figure A-1 is a schematic diagram of the bridge circuit for the long-term null stability tests. At the beginning of a test run ($t = 0$) Z_2, Z_4, and Z_6 should be adjusted so that the voltage drops across Z_1, Z_2, Z_3 (Cell I), Z_4, Z_5 (Cell II), and Z_6 are all equal to $\frac{1}{2}E$. This makes $V_1 = V_2 = 0$ at the beginning of the test. The variation of V_1 and V_2 may then be taken as a description of the drift of the photocells as outlined below.

For this derivation we will need two approximations:

$$Z_7 \approx \infty \tag{1}$$

$$dZ_3 \ll Z_3 \tag{2}$$

The equation for Loop 1 is

$$V_1 = \frac{E}{2} - \frac{EZ_3}{Z_3 + Z_4} \tag{3}$$

Taking the derivative

$$\frac{dV_1}{dZ_3} = -\frac{EZ_4}{(Z_3 + Z_4)^2} \tag{4}$$

Using (2), we have

$$Z_3(t) \approx Z_4 \tag{5}$$

Since we started with the initial condition $V_1 = 0$, then

$$dV_1 = V_1 \tag{6}$$

Substituting (5) and (6) into (4) and rearranging terms,

$$\frac{dZ_3}{Z_4} \approx D_1 = -\frac{4V_1}{E} \quad \text{(approximate absolute drift)} \tag{7}$$

where we let D_1 represent the approximate absolute drift obtained from $-4\ V_1/E$. D_1 is called the absolute drift since it is being compared with a wirewound resistor which has negligible drift.

The equation for Loop 2 is

$$V_2 = \frac{EZ_3}{Z_3 + Z_4} - \frac{EZ_5}{Z_5 + Z_6} \tag{8}$$

$$dV_2 = \frac{EZ_4}{(Z_3 + Z_4)^2}\, dZ_3 - \frac{EZ_6}{(Z_5 + Z_6)^2}\, dZ_5 \tag{9}$$

Again, since $V_2 = 0$ at $t = 0$, then $V_2 = dV_2$. Making approximations similar to those above and rearranging terms, (9) reduces to

$$\frac{dZ_5}{Z_5} - \frac{dZ_3}{Z_4} \approx D_2 = -\frac{4V_2}{E} \quad \text{(approximate relative drift)} \tag{10}$$

where we let D_2 represent the approximate relative drift obtained from $-4\ V_2/E$.

We shall now investigate the error introduced by employing the approximations shown in (1) and (2). To obtain the error introduced by assuming that the input impedance of the recorder is infinite, let us assume that it has a finite resistance, Z_7. For this derivation, let us assume the same initial bridge adjustments as those used for the test run described above. Then, $Z_2 = Z_1$. Writing node voltage equations for V_a and V_b.

$$\frac{V_a - E}{Z_3} + \frac{V_a - V_b}{Z_7} + \frac{V_b}{Z_1} = 0 \tag{11}$$

$$\frac{V_b - E}{Z_1} + \frac{V_b - V_a}{Z_7} + \frac{V_b}{Z_1} = 0 \tag{12}$$

Solving (11) and (12) for V_a and V_b:

$$V_a = \frac{2EZ_4\ Z_7^2 + EZ_4\ Z_7\ (Z_1 + Z_3)}{2Z_7^2\ (Z_3 + Z_4) + Z_7\ (Z_1\ Z_3 + Z_1\ Z_4 + 2Z_3\ Z_4)} \tag{13}$$

$$V_b = \frac{EZ_7^2\ (Z_3 + Z_4) + EZ_4\ Z_7\ (Z_1 + Z_3)}{2Z_7^2\ (Z_3 + Z_4) + Z_7\ (Z_1\ Z_3 + Z_1\ Z_4 + 2Z_3\ Z_4)} \tag{14}$$

The voltage reading shown on Recorder A is $V_a - V_b$, or from (13) and (14)

$$V_1 = V_a - V_b$$

$$= \frac{E(Z_4 - Z_3)}{2(Z_3 + Z_4) + \frac{1}{Z_7}(Z_1 Z_3 + Z_1 Z_4 + 2Z_3 Z_4)} \qquad (15)$$

We shall now use the approximation shown in (5). The error introduced by this assumption is derived later and will be shown to be very small for a small measured drift. This approximation is acceptable for this illustration. Since we also know that

$$Z_3 - Z_4 = \Delta Z_3 \qquad . \qquad (16)$$

substituting (5) and (16) into (15),

$$V_1 \approx \frac{-E(\Delta Z_3)}{4Z_4\left(1 + \frac{Z_1 + Z_4}{2Z_7}\right)}$$

or

$$\frac{\Delta Z_3}{Z_4} = \frac{-4V_1}{E}\left[1 + \left(\frac{Z_1 + Z_4}{2Z_7}\right)\right] \qquad (17)$$

For the original assumption where $Z_7 \to \infty$, we see that (17) does indeed reduce to (7).

To calculate the error introduced by the approximation quoted in (2), let us assume that the input impedance of the recorders are essentially infinite and begin with (3).

$$V_1 = \frac{E}{2} - \frac{EZ_3}{Z_3 + Z_4} \qquad (3)$$

$$= -\frac{E}{2}\left[\frac{Z_3 - Z_4}{Z_3 + Z_4}\right] \qquad (18)$$

If we let ϵ_1 equal the true absolute drift in Z_3 (Photocell I) which has occurred since t = 0, we know that

$$Z_3 = (1 + \epsilon_1)\, Z_4 \qquad (19)$$

where ϵ_1 may be either positive or negative depending on the direction of the drift. Substituting (19) into (18) and solving for ϵ_1,

$$\epsilon_1 = \frac{-4\frac{V_1}{E}}{1 + 2(\frac{V_1}{E})} \tag{20}$$

Combining (7) and (20),

$$\epsilon_1 = \frac{2D_1}{2 - D_1} \tag{21}$$

This expression gives the true absolute drift in terms of the absolute drift computed from (8). The error, δ, introduced by using (7) instead of (21) is

$$\delta = \epsilon_1 - D_1 = \frac{D_1^2}{2 - D_1} \tag{22}$$

Examining (21) more closely, we see that if the drift is small, $2 - D_1 \approx 2$ and (21) reduces to $\epsilon_1 \approx D_1$. Equation (20) is the final expression which should be retained for calculating the true absolute drift directly from the recorder output.

Extending this analysis to include the relative drift, consider (8)

$$V_2 = \frac{EZ_3}{Z_3 + Z_4} - \frac{EZ_5}{Z_5 + Z_6} \tag{8}$$

If we let ϵ_2 represent the true absolute drift in Z_5 (Photocell II) which has occurred since t = 0, we know that

$$Z_5 = (1 + \epsilon_2)\, Z_6 \tag{23}$$

Substituting (19) and (23) into (8)

$$V_2 = \frac{(\epsilon_1 - \epsilon_2)\, E}{(2 + \epsilon_1)\,(2 + \epsilon_2)} \tag{24}$$

Combining (7) and (10) with (24) and solving for ϵ_2,

$$\epsilon_2 = \frac{2(D_1 + D_2)}{2-(D_1 + D_2)} \tag{25}$$

This expression gives the true absolute drift of Photocell II in terms of the approximate drifts calculated from (7) and (10). Combining (21) and (25) the true relative drift is then

$$\epsilon_r = \epsilon_2 - \epsilon_1$$

$$= \frac{4D_2}{(2 - D_1)\,[2 - (D_1 + D_2)]} \tag{26}$$

in terms of D_1 and D_2. If the drifts are small, $(2 - D_1)\,[2 - (D_1 + D_2)] \approx 4$ and (26) does indeed reduce to

$$\epsilon_r \approx D_2 \qquad (\epsilon_1,\ \epsilon_2 \text{ small}) \tag{27}$$

The true relative drift may be determined directly in terms of the outputs of the recorders. Substituting (7) and (10) into (26),

$$\epsilon_r = \frac{-4\,(\frac{V_2}{E})}{(1 + 2\,\frac{V_1}{E})\,(1 + 2\,\frac{V_1}{E} + 2\frac{V_2}{E})} \tag{28}$$

If the true absolute drift of Photocell I has already been calculated, (28) may be modified to

$$\epsilon_r = \frac{(\frac{V_2}{V_1})\,\epsilon_1}{(1 + 2\,\frac{V_1}{E} + 2\,\frac{V_2}{E})} \tag{29}$$

Correction factors obtained from these equations for the data given in Section 4 are negligible. The data may be assumed to be the true relative and absolute drifts.

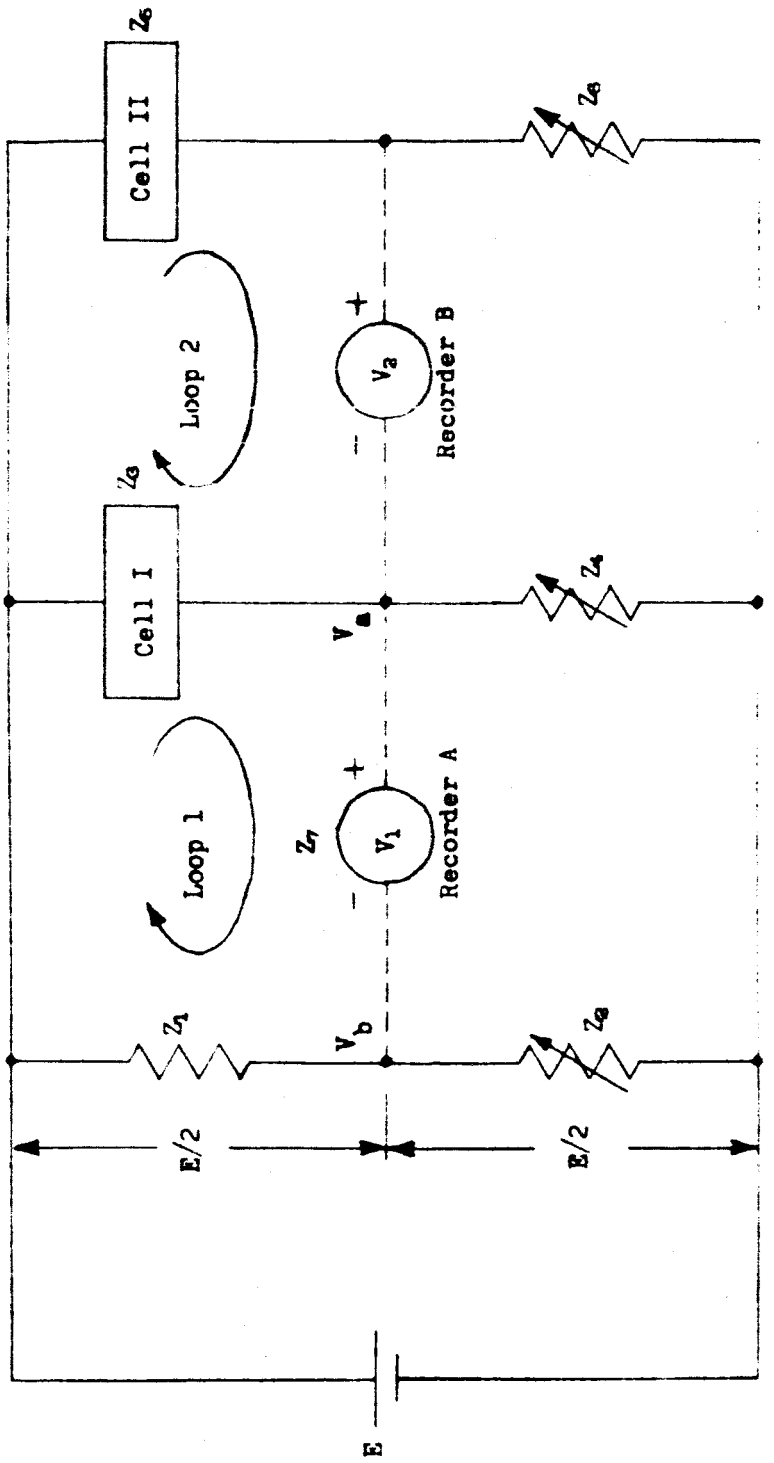

Figure A-1. Bridge Circuit